

Monitoring the Land Subsidence in Kolkata district using High-Resolution Sentinel-1A SAR data

*The Dissertation is submitted in partial of the requirements for the degree of Master of
Science in Remote Sensing and GIS at Vidyasagar University*

By

Amit Bhunia

Roll No – VU/PG/22/34/02-IVS-0006

Reg. No. – 1220610

Year – 2019-2020

Under the supervision of

Dr. Jatisankar Bandyopadhyay

Associate Professor and HOD, Vidyasagar University



Department of Remote Sensing and GIS

Vidyasagar University

Midnapore, 721102

Paschim Medinipur, West Bengal



Office of the Department of Remote Sensing & GIS
Vidyasagar University, Midnapore
Paschim Medinipur- 721102
Telephone: office (03222)2766544/276555/276558
Email: hod_rsgis@mail.vidyasagar.ac.in

Ref. no. VU/RSGIS/Admin/ /2024

Date:

CERTIFICATE

This is to certify the dissertation entitled as, “**Monitoring the Land Subsidence in Kolkata district using High-Resolution Sentinel-1A SAR data**” is a bona fide record of the project work undertaken and completed by **Amit Bhunia** under my guidance and supervision during the academic session 2022-2024, submitted before Vidyasagar University, Paschim Midnapore, for the partial fulfilment of the degree of M.Sc. in Remote Sensing and GIS.

.....
.....
Signature of the Student
(Amit Bhunia)

(Dr. Jatisankar Bandyopadhyay)
Dissertation advisor
Department of Remote Sensing and GIS
Midnapore: 721102
Dist.: Paschim Medinipur
West Bengal, India

Declaration

I, hereby certify the field work report entitled "**Monitoring the Land Subsidence in Kolkata district using High-Resolution Sentinel-1A SAR data**" has been submitted for the partial fulfilment of M.Sc. degree in Remote Sensing and GIS from Vidyasagar University, is an original place of research work carried out by me under the supervision of **Dr. Jatisankar Bandyopadhyay**, Head, Department of Remote Sensing and GIS, Vidyasagar University, Midnapore, West Bengal. The work has not been submitted any other institute for any degree or diploma. Wherever I have used materials (Data, Theoretical Analysis, Figure, and Text) taken from the other sources, I had given due to credit to them by citing them in the text of the work and giving their details in the reference.

Date: 08-07-2024

Place: Dept. of RS and GIS

(Amit Bhunia)

Registration No: 1220610 of 2019- 2020

Roll: VU/PG/22/34/02-IVS-0006

Department of Remote Sensing and GIS,

Vidyasagar University

Midnapore- 721102

West Bengal, India

Acknowledgement

At first, I would like to offer my sincere gratitude to my parents for their constant inspiration and encouragement during the project work.

I would like to thank my respected guidance and supervisor, **Dr. Jatisankar Bandyopadhyay**, Head of the Department of Remote Sensing and GIS, Vidyasagar University, Midnapore, West Bengal, for his constant support. Hereby, I thank him for his patience and supervision to complete my project on "**Monitoring the Land Subsidence in Kolkata district using High-Resolution Sentinel-1A SAR data**"

I am also greatly thankful to **Dr. Dipanwita Dutta** and **Dr. Nirupam Acharyya**, Assistant Professor in the Department of Remote Sensing and GIS, Vidyasagar University, Midnapore for their kindly help to complete my dissertation work.

I would like to thanks **Mr. Sikhendra Kisor De** (Visiting Faculty, Vidyasagar University, Midnapore, and Retired Director of Geo-physics (Geological Survey of India) for his co-operation, constructive comments and support.

I would also like to express my deepest gratitude to **Mr. Suman Das**, Research Scholar, Department of Remote sensing and GIS, Vidyasagar University, and **Mr. Avik Saha** and **Ms. Rali Hansda** (Research Scholar, RS and GIS), **Subhadip Barman** and **Lal Mohammad** (Research Scholar, Centre for Environmental Studies) for their excellent guidance, encouragement, patience and personal attention during every step of my project work.

Special thanks to our Laboratory technician **Mr. Sumanta Saha** and **Aslam Khan**.

My Special thanks to my classmates & friends for their kind co-operation during the course of investigation.

Place: Midnapore

Signature:

Date: 08-07-2024

Table of Contents

Abbreviations:	1
Abstract:	2
1 Introduction:	3
1.1 Background of the study	4
1.2 Statement of Problem.....	5
1.3 Research Question	6
1.4 Aim	6
1.5 Objectives	6
1.6 Scope of the study:.....	6
1.7 Significance of the Study	7
1.8 Organization of the Thesis	7
2 Literature Review:	9
2.1 Previous Incidence of Land Subsidence:	9
2.2 RADAR System Geometry:.....	12
2.3 Synthetic Aperture Radar (SAR):	13
2.4 Interferometric Synthetic Aperture Radar (InSAR):.....	15
2.5 Persistent Scatterer Interferometric Synthetic Aperture Radar (PSInSAR):.....	16
Phase Unwrapping	17
3 About the Study Area:	18
3.1 Physical Characteristics of the study area.....	18
3.1.1 Topography:	18
3.1.2 Climate of Kolkata:.....	19
3.1.3 Geology and Geomorphology of Kolkata:.....	20
3.1.4 Lithology:.....	21
3.2 Socio-economic characteristics:.....	22
3.2.1 Population:	22
3.2.2 Transport and Communication:	22
4 Materials and methods:	23
4.1 Materials	23
4.1.1 Sentinel-1 SLC Data:.....	23
4.1.2 Sentinel 2A data:.....	24
4.1.3 SRTM data:.....	24
4.1.4 Opensource software packages:.....	25

Contents

4.1.5	Matlab software:	25
4.2	Methodology	26
4.2.1	Data pre-processing:	26
4.2.2	Data processing:.....	29
4.2.2.1	Data pre-processing with snap2stamps	29
4.2.2.1.1	Secondaries or slave images preparation:	29
4.2.2.1.2	Master image preparation:.....	30
4.2.2.1.3	Splitting the secondaries or slave images:.....	30
4.2.2.1.4	Coregistration and interferogram generation:	31
4.2.2.1.5	StaMPS Export:.....	33
4.2.2.2	Data processing through StaMPS in Matlab	33
4.2.2.2.1	Step -1: Load the data.....	34
4.2.2.2.2	Step -2: Estimate Phase Noise.....	34
4.2.2.2.3	Step -3: PS selection.....	35
4.2.2.2.4	Step -4: PS weeding	36
4.2.2.2.5	Step -5: Phase Correction.....	37
4.2.2.2.6	Step -6: Phase Unwrapping:.....	37
4.2.2.2.7	Step- 7: Estimate spatially-correlated look angle (DEM) error:	41
4.2.2.2.8	Step -8: Atmospheric Filtering:	42
5	Result and Discussion:.....	43
5.1	PS-InSAR trend analysis without removing any error	44
5.2	PSInSAR trend analysis with removing all the errors	47
5.3	Zone-wise land upliftment and subsidence analysis during 2019-2024	49
a)	Gardenreach:.....	49
b)	Cossipore:	50
c)	Science City:.....	51
d)	Mukundapur:	51
e)	Thakurpukur:	51
f)	Barabazar:.....	52
6	Conclusion:.....	56
Reference:	58

Table of Figures:

Figure 1.1: Locations of land subsidence regions in the world	4
Figure 1.2: Locations of subsidence areas in different states of India.....	5
Figure 2.1: RADAR Geometry	13
Figure 2.2: The Electromagnetic Spectrum with Microwave region.....	14
Figure 2.3: Sensitivity of SAR measurements to forest structure and penetration into the canopy at different wavelengths used for airborne or spaceborne remote sensing observations of the land surface.....	15
Figure 2.4: Interferometric Synthetic Aperture Radar (InSAR) process	15
Figure 2.5: Process of PSInSAR.....	17
Figure 3.1: Location map of the study area	18
Figure 3.2: Elevation map of Kolkata district.....	19
Figure 3.3: Geomorphology of Kolkata district.....	21
Figure 3.4: Lithology of Kolkata district	22
Figure 4.1: Ascending and Descending orbit of Sentinel-1 SAR images	23
Figure 4.2: Methodological Workflow for PSInSAR integration with StaMPS	26
Figure 4.3: Process of Finding Master and Slaves or Secondary Images	27
Figure 4.4: Image acquisition graph with their Perpendicular and Temporal Baseline.....	28
Figure 4.5: Shorting and storing the Secondaries or Slaves image according to the dater.....	30
Figure 4.6: Sentinel 1 SLC image IW (Interferometric Wide) swath graph and 2 IW swath created by the Master Image splitting graph.....	30
Figure 4.7: All Slaves images split through graph 3 in Snap2stamps.....	31
Figure 4.8: StaMPS exported file screenshot which is used in the PSInSAR process	33
Figure 4.9: Principal of Phase Unwrapping	38
Figure 4.10: Date-wise wrapped interferograms	39
Figure 4.11: Date-wise all Unwrapped interferograms.....	39
Figure 5.1: Date-wise LOS Velocity without removing any error (06-02-2019 to 04-02-2024)	46
Figure 5.2: Date-wise LOS velocity with removed all type of error	48
Figure 5.3: PS points of LOS velocity a) Gardenreach b) Cossipore c) Science City d) Mukundapur e) Thakurpukur f) Barabazar	50
Figure 5.4: Showing the major land subsidence area in Kolkata district.....	53
Figure 5.5: Areas in the Kolkata district where Land Subsidence detected.....	55

List of Graphs:

Graph 1: Last 10 years rainfall data graph.....	20
Graph 2: Master Image Splitting Graph.....	30
Graph 3: Secondaries or Slave Image splitting processing graph.....	31
Graph 4: Coregistration and interferogram generation methodology graph.....	32
Graph 5: Date-wise LOS velocity without removing any error.....	45
Graph 6: Mean LOS velocity with all errors removed	49
Graph 7: Major 6 location's LOS displacement graph	54

List of Tables:

Table 1: Previous Literature Review the Studies Land Subsidence in different region in India	12
Table 2: SAR band with their frequency and wavelength	14
Table 3: Monthly rainfall of Kolkata district from 2013 to 2022 (last 10 years).....	20
Table 4: Sentinel 2A satellite Bands with their central wavelength and Spatial resolution.....	24
Table 5: Master and Slaves or Secondary image with their Acquisition date, Temporal Baseline, Perpendicular Baseline.....	28
Table 6: controlling parameters of Estimation Phase noise	35
Table 7: Controlling factors of PS Point selection.....	36
Table 8: PS Weeding controlling factors	37
Table 9: Phase Correction controlling factors.....	37
Table 10: Phase Unwrapping controlling factors	40
Table 11: Estimate Spatially-Correlated Look Angle Error controlling factors	41
Table 12: Sentinel-1 images with their Perpendicular baseline (meters) and Temporal baseline (days) respectively.	43
Table 13: Date-wise Mean LOS velocity without any error removed.....	44
Table 14: Date-wise LOS velocity value with removal of all errors like DEM error, Tropospheric error, Orbit error.....	47

Abbreviations:

ADI	Amplitude Dispersion Index
ALOS	Advanced Land Observing Satellite
APS	Atmospheric Phase Screen
ASI	Amplitude Stability Index
CARTOSAT-1	Cartography and Satellite
CGWB	Central Ground Water Board
DEM	Digital Elevation Model
DInSAR	Differential Interferometric Synthetic Aperture Radar
ENVISAT	Environmental Satellite
ERS	European Remote Sensing
GNSS	Global Navigation Satellite System
GIS	Geographic Information system
InSAR	Interferometric Synthetic Aperture Radar
ISRO	Indian Space Research Organization
LOS	Line of Sight
PS	Persistent Scatterer
PSI	Persistent Scatterer Interferometry
PSInSAR	Persistent Scatterer Interferometric Synthetic Aperture Radar
RADAR	Radio Detection and Ranging
RADARSAT	Radio Detection and Ranging Satellite
SENTINEL	Copernicus satellite constellation by the European Space Agency
SRTM	Shuttle Radar Topography Mission
SWIR	Short-wave Infrared
TerraSAR-X	Terra Synthetic Aperture Radar X-band
ESA	European Space Agency
GPS	Global Positioning System
GSI	Geological Survey of India
AOI	Area of Interesting
SBAS	Small Baseline Subset
SAR	Synthetic Aperture Radar
StaMPS	Stanford Method for Persistent Scatterers
$\Delta\phi$	Phase difference
TOPS	Terrain Observation with Progressive Scans
VV	Vertical-Vertical Polarization

Abstract:

Land subsidence is considered a threat to developing cities and is triggered by several natural (geological and seismic) and human (mining, groundwater withdrawal, oil and gas extraction, and construction) factors. This study has been made to estimate the land subsidence over the at Kolkata district using the PSInSAR technique. Sentinel-1A Synthetic Aperture Radar (SAR) data from 2019 to 2024 was applied to investigate the land subsidence as well as land upliftment. From PSInSAR techniques, this area significantly extracted the Line of Sight (LOS) displacement from the Permanent Scatter (PS) point. The overall process was done in the SNAP, Snap2stamps, StaMPS, and MATLAB software, respectively. The subsidence result showed that the areas under Gardenreach, Cossipore, Thakurpukur, Mukundapur, Science City, and Barabazar were highlighted as subsiding zones over this study area. The maximum subsidence rate is observed as 5.88 mm/year during 2019-2024. This area subsided due to the overexploitation of groundwater, rapid urbanization, soft soil composition, poor drainage and water management, underground construction, riverine and coastal processes, seismic activity, sediment displacement, and also other anthropogenic factors. The influencing areas for land subsidence are Behala, Nayabad, Dum Dum, Paikpara, and Topsia which are showing alarming rates of subsidence. The findings suggested that a comparison between land subsidence-affected areas and piezometric level change in those areas confirms the reason for subsidence in those regions. Therefore, extraction of groundwater should be restricted by proper planning and policy implementation in all parts of the city to manage the problems due to land subsidence.

Keywords: Land Subsidence, Kolkata, InSAR, PSInSAR, Sentinel-1, StaMPS, SNAP, Snap2stamps.

Chapter – 1

Introduction

1 Introduction:

Subsidence refers to the downward vertical movement of the Earth's surface, which can result from natural processes or human activities (Bagheri-Gavkosh et al., 2021; Motagh et al., 2008). Subsidence primarily involves vertical movement and is distinct from horizontal slope movement. Land subsidence is the continuous or unexpected sinking of the Earth's surface caused by the movement of subsurface elements. It is often caused by the over-extraction of water, oil, natural gas, or minerals through activities such as pumping or mining. Groundwater extraction is causing soil subsidence in several nations, including the USA, UK, Australia, China, Egypt, France, Germany, India, Iran, Italy, Japan, Mexico, Poland, Saudi Arabia, Sweden, and the Netherlands, etc.

Space-borne subsidence monitoring has emerged as a superior technique following the development of the Interferometric Synthetic Aperture Radar (InSAR) technique. It can measure deformation on the surface for over a range of days to years. The innovation of radar interferometry has elevated the imaging-based subsidence monitoring techniques to an entirely different level due to its capacity of synoptic coverage, atmospheric condition independence, the flexibility of any-time observation, and high accuracy. Such imaging techniques have reduced the danger and the costs associated with conventional methods, which require extensive fieldwork

The Synthetic Aperture Radar (SAR) hovers over a particular area at regular intervals and takes images of the spot at a very high spatial resolution. The InSAR technique acquires two three-dimensional images of the Earth's surface from two slightly different positions (spatial baseline). When images are acquired at different times (temporal baseline), using the Differential SAR Interferometry (DInSAR) technique, it is possible to measure the changes in the surface topography. These measures are shown by a series of colored bands, also known as fringes or interferograms.

To detect land deformities up to the sub-centimeter scale, one had to rely on radar images of the area under investigation, acquired at different temporal baselines, before the development of the DInSAR technique. However, notwithstanding the advantages, the conventional DInSAR technique has certain limitations, such as i) small spatial baseline as less than 200 m, ii) baseline dependent accuracy of external Digital Elevation Model (DEM), iii) Atmospheric effects, iv) Temporal and geometric decorrelation, etc. ((Raspini et al., 2013; Zebker & Villasenor, 1992) Out of these, temporal decorrelation is considered the main factor behind the data loss at the subsidence zone.

Ferretti et al. (2000) presented the Persistent Scatterer Interferometric Synthetic Aperture Radar (PSInSAR) technique to overcome the limitations of the conventional DInSAR technique. This technique distinguishes deformations in the land topography even at the millimeter level. The PSInSAR technique is a geodetic SAR Interferometry technique that utilizes at least two SAR images to produce maps of topography or distortion of the Earth's surface (Ferretti et al., 2001a; Hooper et al., 2012a; Kampes, 2006; Prati et al., 2010). The satellite-based PSInSAR technique can determine the surface deformation with sub-millimeter accuracy using the C-band Sentinel-1 data. By obtaining time-series SAR information (Crosetto et al., 2016), the PSInSAR

technique decreases temporal and geometric decorrelation by selecting stable Persistent Scatterers (PS) point, which are geometrically accurate, by obtaining time-series SAR information (Crosetto et al., 2016). Moreover, PSInSAR can diminish atmospheric interference by using multi-temporal time-series SAR information with PSs (Davila-Hernandez et al., 2014; Ferretti et al., 2001a)

The PSInSAR technique is increasingly adopted in the over-exploration of ground-water areas to detect land deformation using the C-Band data. C-band SAR data has a larger possibility of temporal decorrelation than L-band data since it is limited to a spatial and temporal baseline. The present study detected a slow process of subsidence in Kolkata city due to the over-exploration of groundwater. The short wavelength C-band is more suitable for detecting this subsidence if the optimal baseline is maintained. On the other hand, the long-wavelength L-band can effectively detect rapid subsidence (Chatterjee et al., 2015a).

1.1 Background of the study

Land Subsidence is the gradual and downward movement of the Earth's surface. In other words, it is a slow settling or unexpected sinking of the Earth's surface because of the displacement of sub-surface Earth materials. It happens due to mining, and extraction of groundwater, oil, and gas. Land subsidence is evidence of shallow or profound underground disfigurement set off by different sub-surface cycles (Tomás et al., 2014). The first instance of land subsidence was recorded in the marshes of Tokyo in 1924 on account of extract leveling to assess the post-seismic crustal aggravation after the Kanto Earthquake of 1923 (Inaba et al., 1970). Since then, around 150 incidents of urban land subsidence of significance have been noted (Heath and Spriull 2003). More than 44,000 square kilometers of the area have been affected by land subsidence in the United States alone. Out of this, around 80% happened due to indiscriminate extraction of groundwater. Similarly, many regions in Europe have been experiencing subsidence related to groundwater extraction for quite a long time as reported by the United States Geological Survey (USGS 2017). Risk Assessment is a regular exercise to identify and evaluate the potentials of environmental and artificial disasters to earmark the primary risk factors and, thereby, analyze the possible negative impacts on individuals and nature as mentioned in the European Commission Report (ECR 2010). The ECR 2010 indicates that the subsidence occurred in the United States of America (USA), Spain, Italy, Iran, China, Australia, India, and many other countries, as shown in Figure 1.1

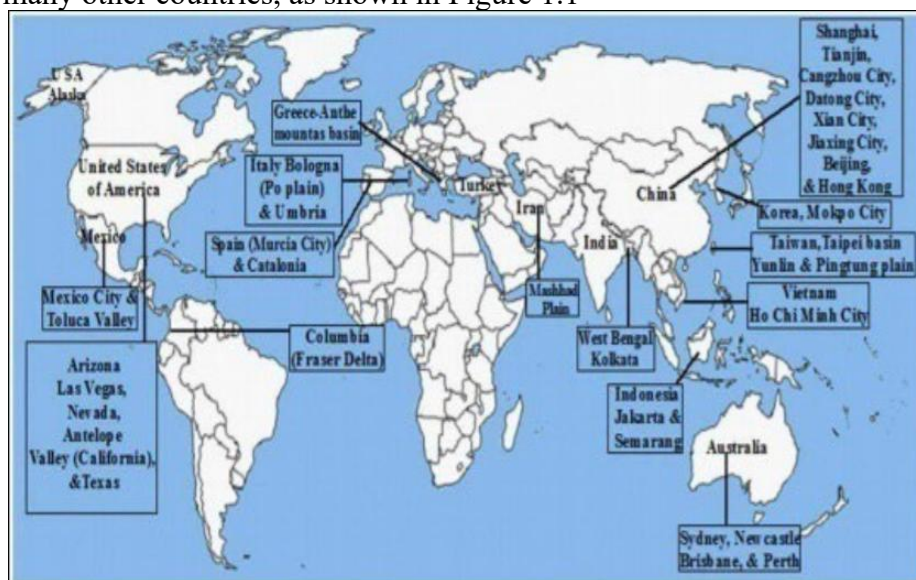


Figure 1.1: Locations of land subsidence regions in the world

Source: (European Commission Report 2010)

In India, several states, i.e., West Bengal, Jharkhand, Bihar, Uttar Pradesh, Gujarat, and Andhra Pradesh, get affected by land subsidence. Figure 1.2 shows the locations where the incidence of land subsidence is frequently reported in India. A study conducted by the Central Ground Water Board (CGWB), Lucknow, Uttar Pradesh, predicted significant land incident subsidence is likely to occur in areas around Lucknow, such as Narhi Charbagh, Rajajipuram, and Gomtinagar, by 2026 due to over-exploitation of groundwater. The study recommended immediate steps to increase water recharge to prevent any severe disaster in the future. Again, land subsidence due to natural gas exploitation has been observed in the Krishna and Godavari deltas in Andhra Pradesh (Rasheed & Dayal, 2012). Here the different locations in India that detect Land subsidence due to different phenomena like Groundwater over-extraction, Coal extraction, Oil and Gas extraction, and Hydrocarbon extraction are shown in Figure 1.2. Land Subsidence by Groundwater over-extraction is detected in Lucknow, Kolkata, Siliguri, etc.

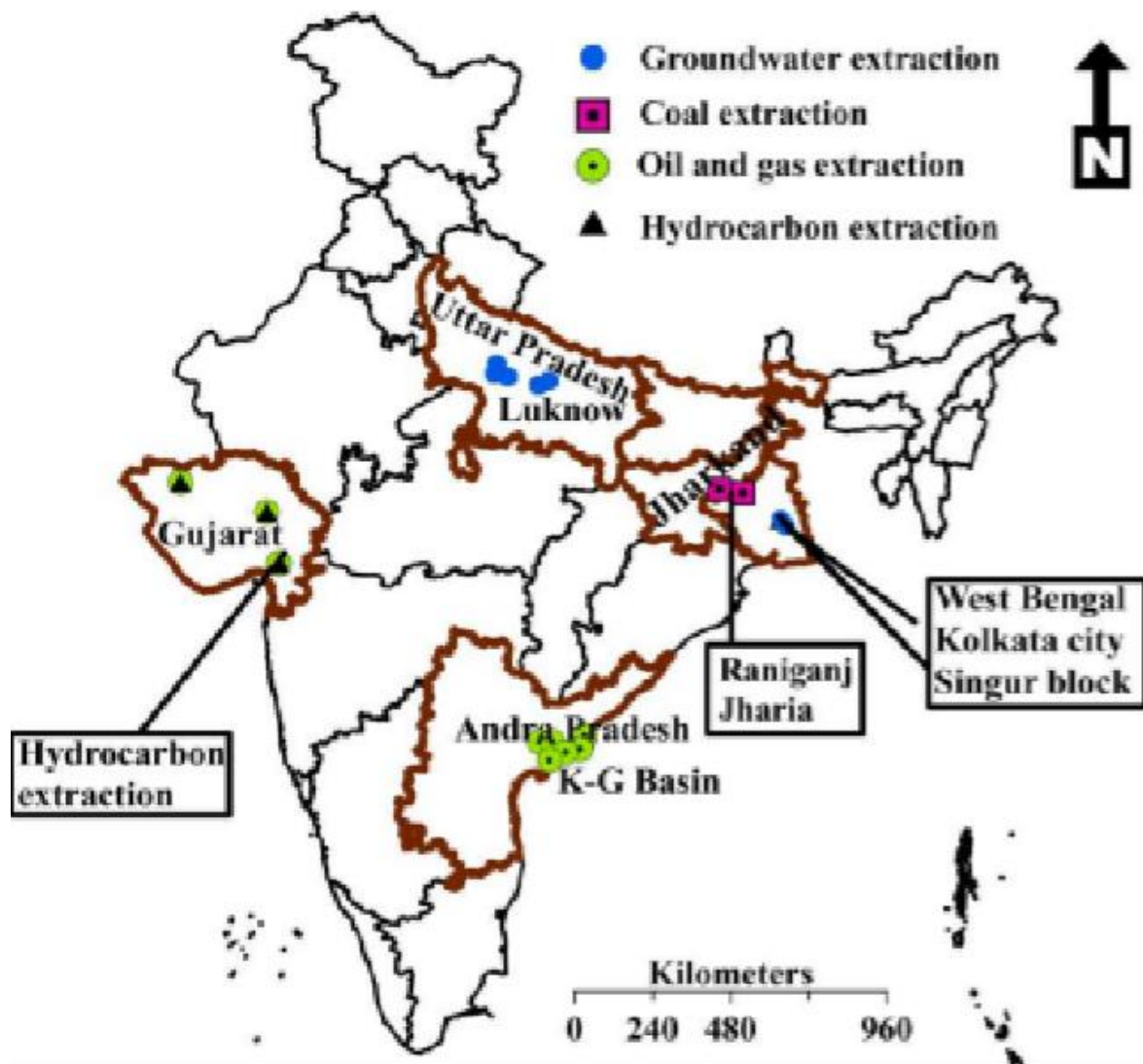


Figure 1.2: Locations of subsidence areas in different states of India

Source: (Ashish Aggarwal & Kumar Srivastava Dharmendra Kumar Gupta Chatterjee, 2020)

1.2 Statement of Problem

In the past, Kolkata has posed a threat to land subsidence, and worsening conditions is underway. However, there are only little public attentions. Although SAR methods have many

advantages, most previous studies concentrated on temperate zone. While in urban areas, there are several confounding factors, such as dense built-up coverage and unstable house structures. Therefore, only using single technique or track may be unable to achieve an accuracy measurement, we must integrate various techniques. Meanwhile, another problem is using different technique and track to calculate LOS deformation. Because of special imaging principle of SAR images, most conventional 3D decomposition methods also have some issues need to be addressed.

1.3 Research Question

Synthetic Aperture Radar (SAR) sensors are playing a significant role in retrieving topographic information, which has been successfully applied in those areas with less vegetation, less agriculture land, high dense settlement area, and tropical climate. However, fewer studies focus on these tropical developed megacities like Kolkata which covered by dense built-up area. In addition, how to select adequate polarization modes for SAR radar images is an important issue. More importantly, it is crucial to know how to effectively extract Line of Sight (LOS) subsidence using PSInSAR and integration of StaMPS approach. Therefore, this research developed to better understand the statuses of land subsidence in this study area, the research question of this study are:

Question-1: Are these SAR images effective for land subsidence monitoring?

Question-2: How to minimize the errors of SAR based results during data processing through PSInSAR with integration of StaMPS techniques?

Question-3: Does over-exploration of groundwater affect Land Subsidence in major urban areas in India?

1.4 Aim

The main aim of this study is “**Monitoring Land Subsidence**”.

1.5 Objectives

This research mainly focuses on land subsidence in the Kolkata District to find the different ground-level changes by time series from 2019 to 2024. This research will use Sentinel-1 SLC satellite image and SRTM DEM for coregistration of the master image.

1. To estimate the land subsidence using Sentinel-1A data using PSInSAR Technique,
2. To analyze the reasons for land subsidence in this region,
3. To find the most suitable method that measures the highest accuracy of Land subsidence.

1.6 Scope of the study:

With the fast development of society, land subsidence already became one of the most challenging disasters in recent years in Kolkata. However, little attention has been paid to these phenomena, whether government or the general public. In view of this situation, the present study analyzes land deformation status in Kolkata (within latitudes 22°30' to 22°37'N and longitudes 88°18' to 88°23'E). To this end, this study also demonstrates the ground water depth with potential zone and sea level rise of Ganga that relates to land subsidence, which can help to better understand the effect of land subsidence.

During the study, other limitations are also stipulated for limiting the scope for this study. The scopes are:

- 1) The Sentinel-1A radar images cover from January 2019 to February 2024, and also only Interferometric Wide swath (IW) products are used.
- 2) In this research is used Shuttle Radar Topography Mission (SRTM) digital elevation model (DEM) with 30m in spatial resolution.
- 4) Only Sentinel-1A high-resolution data is used to estimate land deformation. All processing is implemented using SNAP software, Snap2stamps, and the StamPS approach.

1.7 Significance of the Study

Monitoring land subsidence is crucial for the sustainable development of cities. Kolkata, a major megacity in the state of West Bengal, has significantly contributed to the national GDP, construction, and employment. However, due to rapid economic and population growth, the state government must develop infrastructure to support ongoing and planned construction projects, such as reclaimed lands, railway, and metro development. These projects greatly impact the environment and geological stability. This area's unique geographical environment and human intervention make it susceptible to land subsidence. In recent years, the government has invested a significant amount in addressing land subsidence and landslides. Overexploitation of groundwater is a key factor in land deformation in this region. Additionally, sea level rise due to climate change poses a significant challenge for Kolkata, as a large proportion of the population and economic activities are concentrated along the coastlines. This thesis aims to study the land subsidence status in Kolkata megacities using SAR techniques and a machine learning approach. This approach will help create more accurate deformation scenarios and continuous land deformation maps. The PSInSAR method can quantify uncertainties in incomplete or erroneous data by integrating various SAR results. This study suggests that the machine learning-based analysis method can improve the accuracy of land subsidence models and reduce errors in SAR results, ultimately enabling the calculation of vertical deformation rates.

1.8 Organization of the Thesis

The outline of this thesis is shown as follows:

Chapter 1: This chapter introduces the report outlining the background of the study, research status, the specific research objectives, research questions, scope of study, and the significance of this study.

Chapter 2: The second chapter is about literature reviews. In this chapter, the history of SAR radar sensors is first described followed by compared with InSAR. This chapter also indicates the advantages and disadvantages of SAR and InSAR. In addition, the past and present SAR satellites are also listed.

Chapter 3: The third chapter discusses the methodology and its procedures to fulfill the objectives of the research together with an overview of the methodology for validation of results. The principle of the RADAR imaging process, SAR is described in detail in this chapter. In addition, the materials and study areas are also included in this chapter together with the software.

Chapter -1: Introduction

Chapter 4: This chapter provides an overview of the study area with its geographical parameters.

Chapter 5: Chapter 5 is based on the results from Sentinel-1A in the study areas, Then, several sub-areas are selected for further analysis to understand the reasons for land subsidence based on the PSInSAR results. This chapter also discusses the result.

Chapter 6: This chapter contains the conclusion part of the study. And also include the drawbacks and future scope of this study.

Chapter - 2 Literature Review

2 Literature Review:

Land subsidence is an environmental as well as a geological hazard on a global scale. Subsidence has alarmingly risen over the decades due to indiscriminate economic activities and human settlements. This chapter has attempted to gather relevant observations from scholarly works on the background of subsidence activities, subsidence monitoring, early developments in Radio Detection and Ranging (RADAR), etc. Later, the chapter highlights scholarly observations on SAR, InSAR, DInSAR, and PSInSAR technologies.

2.1 Previous Incidence of Land Subsidence:

In a research work (Kumar et al., 2020) about land subsidence in Jharia Coalfield, titled "Land subsidence mapping and monitoring using modified persistent scatterer interferometric synthetic aperture radar in Jharia Coalfield, India". The authors used the Persistent Scatterer Interferometric Synthetic Aperture Radar (PS-InSAR) technique with C Band ENVISAT ASAR data to analyze land subsidence. The study focused on detecting continuous slow-rate subsidence at five major sites in the Jharia Coal Field (JCF). The highest rate of slow deformation among all sites was measured at 29 mm/year, with a total subsidence value of 90 mm.

According to (Aditiya et al., 2017) Surabaya, the second-largest city in Indonesia, has experienced rapid population and industrial growth. The city is facing a potential disaster in the form of land subsidence due to this rapid urbanization. A study titled "Land Subsidence Monitoring by InSAR Time Series Technique Derived From ALOS-2 PALSAR-2 over Surabaya City, Indonesia" used the Interferometric Synthetic Aperture Radar (InSAR) with the Small Baseline Subset (SBAS) technique for time series analysis to investigate land subsidence. The study utilized ALOS-2 PALSAR-2 L band SAR data with ascending orbit. The results of the study showed that subsidence has been observed in several areas of Surabaya, particularly in the northern part, reaching up to approximately 2 cm per year. The study concluded that land subsidence is mainly caused by groundwater consumption for industrial and residential purposes.

This research work (Awasthi et al., 2019) titled "PSInSAR based land deformation based disaster monitoring using sentinel-1 datasets". This paper focused on detecting the Land subsidence in Lucknow district, India. The study used the time series InSAR technique (PSInSAR) in this paper. This research used Sentinel-1 C band SAR data in IW mode with 58 ascending and 59 descending orbit datasets. The overall urban deformation of the Lucknow district is 16 mm/year.

In Kolkata City, land subsidence is occurring due to excessive groundwater extraction. A study titled "Subsidence of Kolkata (Calcutta) City, India during the 1990s as observed from space by Differential Synthetic Aperture Radar Interferometry (D-InSAR) technique" by (Chatterjee et al., 2006). Which used the D-InSAR technique with 4 pairs of C band ERS SAR data with VV polarization. The results indicate that an area in Kolkata City surrounded by Machhua Bazar, Calcutta University, and Raja Bazar Science College experienced subsidence from 1992 to 1998 at an estimated rate of 5 to 6.5 mm/year.

Chapter -2: Literature Review

(Mondal & Paul, 2023) A recent study (Mondal & Paul, 2023) "Monitoring of groundwater-generated land subsidence by persistent scatterer analysis – A case study of the Kolkata Municipal Corporation (KMC), West Bengal" deals with the problem of land subsidence over the city of Kolkata, the state capital of West Bengal. Excessive withdrawal of groundwater resources in the KMC area resulted in land subsidence which was estimated by the Persistent Scatterer Interferometric Synthetic Aperture Radar (PSInSAR) technique. PSInSAR technique estimates the accurate Line Of Sight (LOS) displacement from the points identified as persistent scatterers (PS). The study employed a stack of Sentinel datasets to identify the PS and estimated the temporal rate of ground deformation. The study found that several regions of the city like Gardenreach, Thakurpukur, Behala, Nayabad, Mukundapur, Science City, Dumdum, Paikpara, Cossipore, Central, Barabazar, and Topsia are suffered from severe subsidence. The study area experienced subsidence velocity of 6.4 mm/year during 2014-2020.

In a study titled "Land subsidence analysis using synthetic aperture radar data," researchers (Bokhari et al., 2023) investigated land subsidence in Gwadar City, located in the southwest of Pakistan along the shores of Balochistan. The study utilized a total of 80 Sentinel-1 C band SAR images (40 ascending and 40 descending orbit) between 2017 to 2019 and employed the PSInSAR technique and SARPROZ software. The PS-InSAR results indicated subsidence rates of up to -92 mm/year in the ascending track and -66 mm/year in the descending track in the area of Koh-i-Mehdi Mountain, and up to -48 mm/year in the ascending track and -32 mm/year in the descending track in the area of the deep-sea port.

According to (Blasco et al., 2019) Land subsidence in urban environments is an increasingly prominent aspect in the monitoring and maintenance of urban. This study is titled as "Measuring Urban Subsidence in the Rome Metropolitan Area (Italy) with Sentinel-1 SNAP-StaMPS Persistent Scatterer Interferometry" which focused on monitoring and maintaining Urban infrastructure due to Land subsidence. This research used 82 Descending and 87 Ascending orbit C band Sentinel-1 SAR images with the SNAP-StaMPS PSInSAR technique.

According to (Rafiei et al., 2022) the paper "Aquifer and Land Subsidence Interaction Assessment Using Sentinel-1 Data and DInSAR Technique" investigates the land subsidence due to groundwater extraction in Samalghan Plain of Iran which is exacerbated by climate change and increasing water demand. The study uses DInSAR to analyze the subsidence over 6 years using 25 Sentinel-1 descending SAR images. The analysis shows a clear relationship between groundwater overexploitation and subsidence, the highest average subsidence was in 2019 (34 cm), and the lowest in 2015 and 2018 (18 cm). The study also validated its results using 12 Sentinel-1 ascending images with a correlation coefficient between 0.69 and 0.89 which is acceptable. The results show the direct relationship between extensive groundwater extraction and subsidence. The study suggests that changing cultivation patterns and optimal use of groundwater resources can be practical solutions to mitigate the subsidence effects.

A study titled as "Sentinel-1 for Monitoring Land Subsidence of Coastal Cities in Africa Using PSInSAR: A Methodology Based on the Integration of SNAP and StaMPS" by Cian et al. (2019) investigates urbanization rate effects on surface deformations in sub-Saharan Africa's coastal areas, with focus on Banjul (Gambia) and Lagos (Nigeria). Lack of checks in underground water exploitation, reclamation of wetlands, and growth of built-up areas without proper urban planning have resulted in gross socio-ecosystem imbalances. Employing the Persistent Scatterer Interferometry (PSI) technique using Synthetic Aperture Radar (SAR), this research monitors these land deformation processes with high precision based on the open-

Chapter -2: Literature Review

access Sentinel-1 data. The researchers employed the Stanford Method for Persistent Scatterers (StaMPS) linked to the Sentinel Application Platform (SNAP) to automatically analyse land subsidence which was compared to results obtained from TerraSAR-X, COSMO-SkyMed, and Envisat-ASAR. These findings indicate regions where a lot of soil is shifting, providing valuable information for urban development strategies, disaster risk management, and climate change adaptation interventions. This practice demonstrates that it is necessary to regularly monitor the constantly occurring in such rapidly changing environments to identify any risks and plan for an effective adaptation system.

The paper “Recent advances in SAR interferometry time series analysis for measuring crustal deformation” (Hooper et al., 2012) reviews InSAR for crustal deformation monitoring using PSInSAR and SBAS techniques. Focusing on different parts of the world, the study uses advanced InSAR time series analysis, the Stanford Method for Persistent Scatterers (StaMPS) with data from TerraSAR-X and Envisat-ASAR. Results show much better ground movement detection with high accuracy, useful for earthquake monitoring and volcanic activity assessment. The paper concludes that these advances are good for geophysics and disaster risk management.

According to Kandregula et al. (2024) the research paper "Monitoring deformation in the Himalayan arc using PSInSAR technique" has assessed horizontal and vertical deformation rates in the region of Sikkim and eastern Nepal, areas dominated by strike-slip deformation and having prominent transverse tectonic features. This paper uses Persistent Scatterer Interferometry to process 70 ascending and 78 descending SLC images from February 2017 to August 2023 for measuring displacement along the radar line of sight. Results give way to LOS velocity from -20 mm/year to +15 mm/year, hence indicating important deformation patterns. This research proves the effectiveness of PSInSAR for monitoring geodynamic processes, hence providing insight into risk assessment and management in this geologically active region.

Reference	Study Period	Location	Research Technique	Land Subsidence
(Sikdar et al., 1996)	1956-1993	Selected location in Kolkata Howrah Municipal Corporation zone.	One-dimension consolidation theory	3.33 mm/year to 13.78 mm/year
	1956-1994			
	1958-1993			
(Chatterjee et al., 2006)	1992-1998	Selected locations in Kolkata city	D-InSAR using ERS InSAR data	5 mm/year to 6.5 mm/year
	1956-2000			
	1958-2000			
Bhattacharya (2008)	1956-2005	Selected locations in Kolkata city	Linear and Logarithmic Theory	10.56 mm/year to 20.46 mm/year
	1958-2000			
	1956-2005			
(Sahu & Sikdar, 2011)	1956-2005	Salt Lake City in Kolkata and the east Kolkata wetlands	One-dimension consolidation theory	13.53 mm/year
	1956-2005			

Chapter -2: Literature Review

(Ganguli, 2011)	1998-2002	Singur block, Hooghly district, West Bengal	One-dimension consolidation theory	6.13 mm/year
(Kumar Bhattacharya & Kumar, 2012)	1956-2000	Selected locations in East Kolkata	Linear and Logarithmic Theory	7.50 mm/year
(Suganthi et al., 2017)	2003-2007	Selected locations in Kolkata city	D-InSAR using ENVISAT ASAR data	12 mm/year
	2007-2010			18 mm/year
(Malik et al., 2018)	Sept. 2011 to Nov. 2013	Delhi NCR	PSI using TerraSAR-X data	10 to 32 mm/year
(Tripathi et al., 2018)	Dec. 2014 to Dec. 2015	Rudrapur city, Uttarakhand	PSInSAR using TerraSAR-X data	2.46 mm/ year
(Gupta et al., 2019)	2017-2019	Jagadhri city, Haryana	D-InSAR using Sentinel-1 data	4.89 cm/year
(Tripathi & Tiwari, 2019)	2018-2019	Chandigarh	D-InSAR using Sentinel-1 data	4.98 cm/year
(Suganthi & Elango, 2020)	2003-2010	Salt Lake City in Kolkata	SBAS-InSAR using ENVISAT ASTER data	8 mm/year
(Kadiyan et al., 2021)	2005-2018	Mohali-Chandigarh	DInSAR using ALOS PALSAR-1/2 and RADARSAT data	4 to 7.5 mm/year

Table 1: Previous Literature Review the Studies Land Subsidence in different region in India

2.2 RADAR System Geometry:

The RADAR emits electromagnetic radiation and records its backscattered signal, travel time, and intensity. Returned backscatter intensity contains electrical and geometrical information of the target. Travel time is used to calculate the distance between the RADAR and reflected features. Since radar generates electromagnetic radiation without involving any external source, it can work around the day. It operates in the microwave range of electromagnetic radiation with a longer wavelength and lower frequency than the optical range. The RADAR imaging system is less sensitive to fog, clouds, rain, and snow.

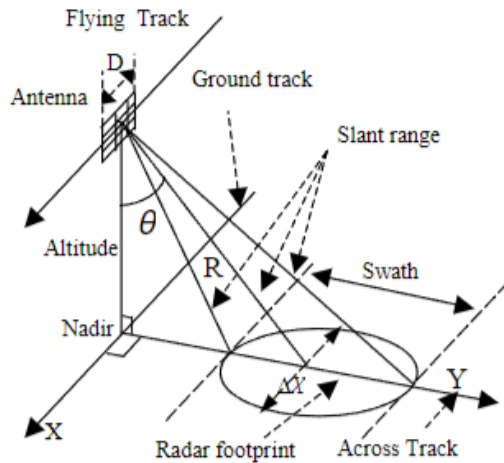


Figure 2.1: RADAR Geometry

Source: Ding et al. (2014)

The information contained in a RADAR image is distinct from optical or infrared images. The most essential factor of imaging RADAR is the use of coherent pulses. The antenna mounted on the platform, transmits RADAR signals as side-looking direction towards the earth's surface. In other words, the imaging is pointed perpendicular to the direction of its movement. RADAR geometry shown in **Error! Reference source not found.**

2.3 Synthetic Aperture Radar (SAR):

The limitation of real aperture radar (RAR) is solved in synthetic aperture radar (SAR) systems. In SAR systems a short physical antenna is used as in RAR, which is synthesized so that it can act as a very long antenna. The result of this mode of operation is a very narrow effective antenna beam width, even at far ranges, without requiring physically long antenna or a short operating wavelength, which increases the azimuth resolution subsequently.

SAR stands for Synthetic Aperture Radar. Synthetic Aperture Radar (SAR) is an active remote sensing system that is usually a space-based remote sensing technique that uses satellites but can also be mounted on aircraft or Unmanned Aerial Vehicles (UAV). SAR has all-weather day and night operational capabilities because it uses microwave region in the Electro Magnetic Spectrum (shows in **Error! Reference source not found.**). The different wavelengths used in SAR are known as bands, such as X, C, L, and P, and different k bands.(Meyer, 2019). SAR bands table with frequency and wavelength described in **Error! Reference source not found.** Table 12

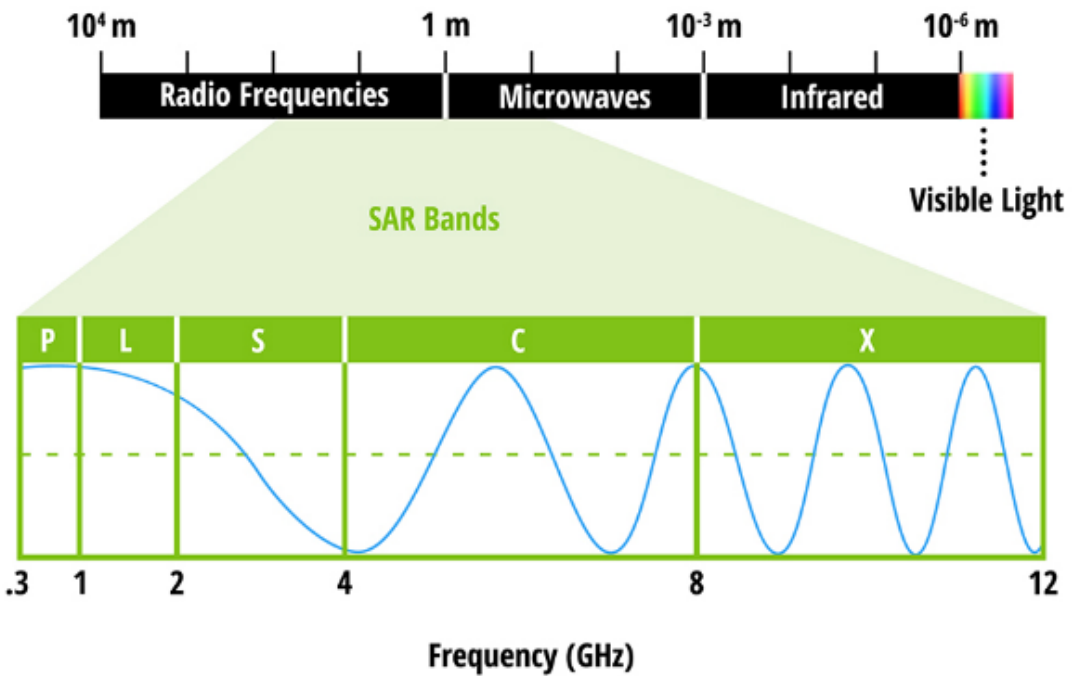


Figure 2.2: The Electromagnetic Spectrum with Microwave region

Source: NASA

Bands	Frequency	Wavelength
Ka	27–40 GHz	1.1-0.8 cm
K	18–27 GHz	1.7-1.1 cm
Ku	12–18 GHz	2.4-1.7 cm
X	8–12 GHz	3.8-2.4 cm
C	4–8 GHz	7.5-3.8 cm
S	2–4 GHz	15-7.5 cm
L	1–2 GHz	30-15 cm
P	0.3–1 GHz	100-30 cm

Table 2: SAR band with their frequency and wavelength

Source: NASA Earth data

Wavelength is the most important feature to consider when working with SAR, as it determines how the radar signal interacts with the earth's surface and how far a signal can penetrate into the medium. This wavelength called as Microwave Band. These microwaves bands are used to illuminate the earth's surface through a radar pulse beam, then the receiving antenna receives the returned signal which is known as backscatter, containing both amplitude and phase components of the wave.

C-band SAR is more effective for slow-rate deformation, while L-band SAR is more suited for quicker subsidence or areas with high levels of vegetation.(Chatterjee et al., 2015b). Sensitivity of SAR measurement to forest structure and penetration into the canopy at different wavelengths and frequencies shown in Figure 2.3.

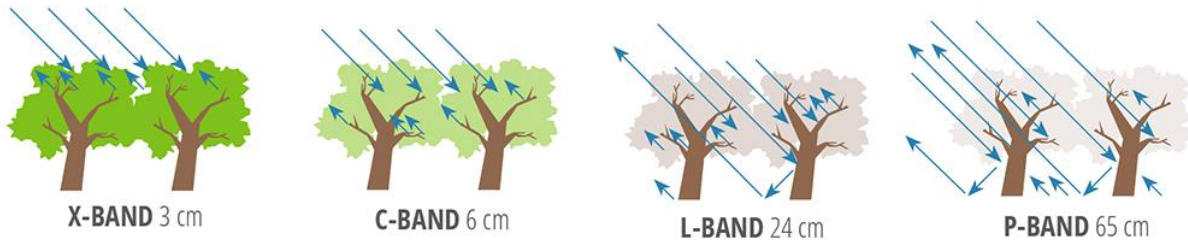


Figure 2.3: Sensitivity of SAR measurements to forest structure and penetration into the canopy at different wavelengths used for airborne or spaceborne remote sensing observations of the land surface Source: NASA

2.4 Interferometric Synthetic Aperture Radar (InSAR):

Interferometric Synthetic Aperture Radar (InSAR), also known as SAR Interferometry, is a technique for measuring changes in ground surface height and movement over time. InSAR works by comparing two RADAR images of the same area taken at different times and measuring the phase shift between them (Chatterjee et al., 2006). When the ground moves, the distance between the sensor and the point changes, causing a corresponding change in the phase value recorded by the sensor. By comparing the phase of two or more radar images, we can determine whether the ground has moved closer to or farther away from the satellite. By combining multiple radar images, we can produce a time history of ground movements with millimeter-level precision. The process of interferometry shown in Figure 2.4

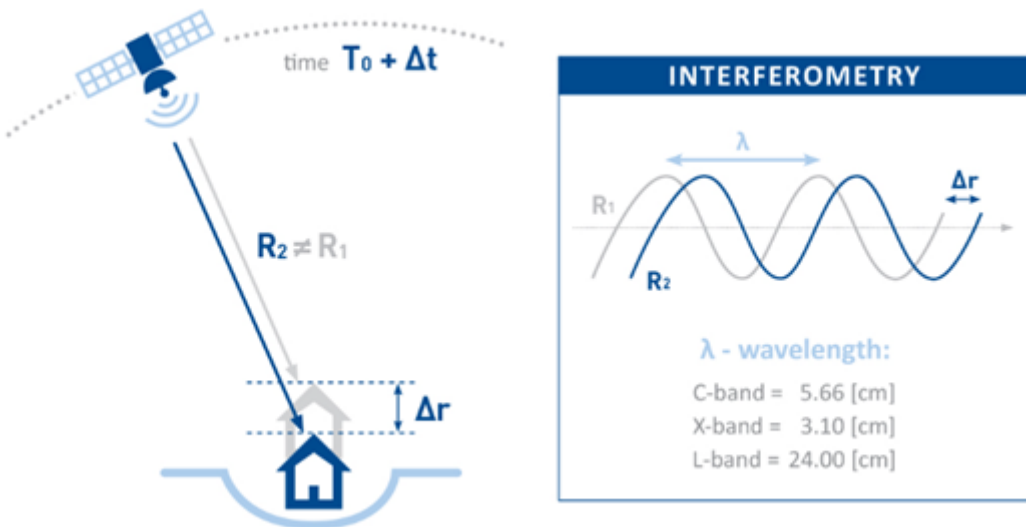


Figure 2.4: Interferometric Synthetic Aperture Radar (InSAR) process

Source: Tre Altamira

The changes in the signal phase, or interferometric phase ($\Delta\varphi$) are expressed by the following equation no 5 (Crosetto et al., 2016):

$$\Delta\varphi = \varphi_1 - \varphi_2 = \frac{4\pi}{\lambda} (R_2 - R_1) \quad 1$$

Where φ_1 and φ_2 are the phases of two SAR images respectively; λ is the wavelength of the SAR band; R_1 is the distance from the SAR to the scatterer by the first acquisition; R_2 is the distance by the second acquisition;

contributions that impact the interferometric phase (φ_{int}) in this 2 (Crosetto et al., 2016):

$$\varphi_{int} = \varphi_{disp} + \varphi_{topo} + \varphi_{orb} + \varphi_{atm} + \varphi_{scat} + \varphi_{noise} + 2\pi k$$

2

where φ_{int} is the interferometric phase, φ_{disp} is the deformation phase due to the deformation in the radar line of sight, φ_{topo} is the topographic phase, φ_{orb} is deterministic flat earth phase and the residual phase signal due to orbit in determination, φ_{atm} is the atmospheric phase, φ_{scat} is the phase resulting from a shift in the earth surface's scatter properties both spatially and temporally between the two observation over time, and φ_{noise} is phase degradation factors, caused by e.g., thermal noise, coregistration noise, and interpolation noise. And k is an integer value called phase ambiguity,

Tropospheric and deterministic flat earth error are removed by SRTM DEM data (Ferretti et al., 2001b; Zebker et al., 1997; Zebker & Goldstein, 1986). This process is happened in StaMPS processing. Flat earth and Topospheric error are removed by this equation

2.5 Persistent Scatterer Interferometric Synthetic Aperture Radar (PSInSAR):

Persistent Scatterer Interferometry (PSI) is a new method developed by the Politecnico di Milano from Italy in 1999, which is an advancement of conventional InSAR techniques. This method is used to study pixels that remain coherent over a sequence of interferograms.

Permanent Scatterers are natural or man-made features that reflect radar waves strongly and consistently. These features can be rock outcrops, buildings, or other rigid structures that remain unchanged over time and with different environmental conditions. (Ferretti et al., 2001b)

This technique is also known as multi-image approach. The term PSI was proposed by the European Space Agency (ESA) to define the second generation of radar interferometry techniques. Nowadays, this term is widely accepted by both the scientific community and the end-users.

Persistent Scatterer Interferometric Synthetic Aperture Radar (PSInSAR) is an advanced technique that has revolutionized the analysis of ground deformation patterns. Unlike conventional InSAR, which uses a limited set of images, PSInSAR uses a multi-image data set consisting of at least 20-25 images. This allows for a more detailed analysis of sub-pixel radar reflections, which in turn enables the removal of atmospheric and orbital errors.

One of the primary advantages of PSInSAR is its ability to identify both linear and non-linear deformation patterns. By analyzing the time histories of movement for every radar target (PS), PSInSAR generates valuable insights. This makes it an invaluable tool for a wide range of applications, including monitoring landslides, subsidence, and ground displacement caused by mining or oil extraction, earthquakes, and other geological hazards. (Colesanti et al., 2002)

In summary, PSInSAR represents a significant evolution in the field of remote sensing, providing a more accurate and detailed analysis of ground deformation patterns. Its ability to generate time histories of movement for every radar target makes it an invaluable tool for a wide range of applications.

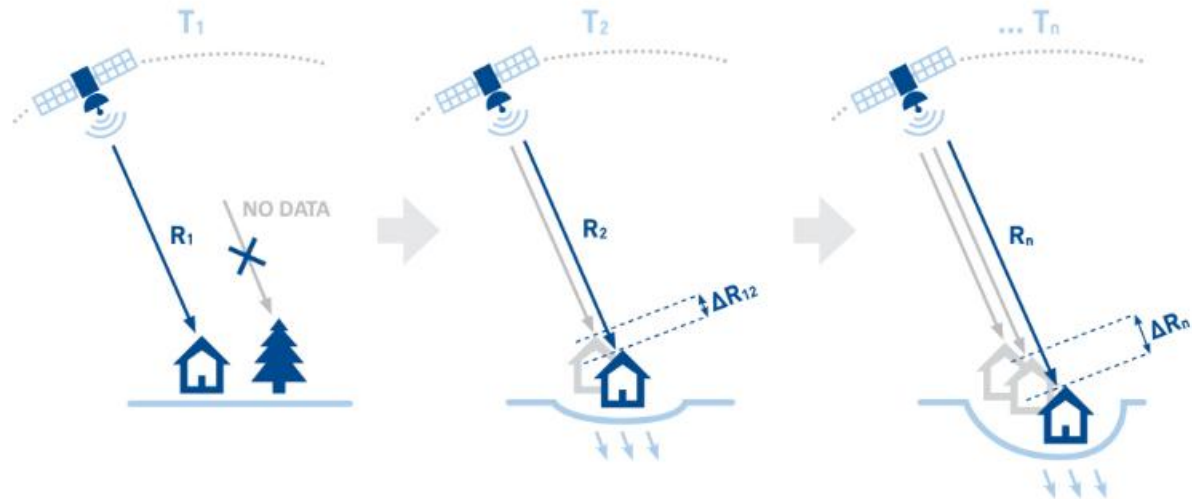


Figure 2.5: Process of PSInSAR

Source: Tre Altamira

Phase Unwrapping

Interferogram filtering is followed by Phase Unwrapping and is the final step for extracting the phase information from the SAR images. Due to the wrapped nature of the phase signal (2π cycles), phase unwrapping must be applied to convert them to one complete cycle and correctly estimate the ground deformation. It involves getting the correct phase from the wrapped phase by removing 2π discontinuities. The interferometric phase of two SAR images at different times can only be measured modulo 2π . This ambiguous phase is known as the wrapped phase. To obtain the complete phase difference from the wrapped phase an integer number of 2π has to be added which can be achieved by adding an exact multiple of 2π to the interferometric phase for every pixel to remove the 2π ambiguity and obtain sequential phase values across the entire image. This results in achieving the values of $-\pi$ or π is achieved depicting a phase jump from one end to the other end. Some of the common algorithms employed for phase unwrapping include Region growing, Minimum cost Flow and Phase decomposition algorithms. In the present study, Minimum Cost flow algorithm was used to perform phase unwrapping of the SAR data pairs.

Chapter -3: Description of the Study area

Chapter – 3 Description of the study area

3 About the Study Area:

Kolkata is the largest metropolitan city in West Bengal and serves as its capital. The city is situated in the eastern part of India, within the latitudes $22^{\circ}30'$ to $22^{\circ}37'N$, and longitudes $88^{\circ}18'$ to $88^{\circ}23'E$. The district is bounded by the North 24-Parganas district in the North, on the South by South 24-Parganas, on the East by North & South 24-Parganas, and on the West by river Hooghly. Kolkata sprawls more or less north-south along the east bank of the Hooghly River within the lower Ganges Delta of eastern India about 75 km (47 mi) west of Bangladesh international border. Kolkata has got Ganga as its main river. The district has an area of approx. 205 sq. Km. Corresponding to 1,84,000 hectares of land which is divided into 16 Boroughs and 144 Wards. According to the results of the census conducted in 2011, the total population of Kolkata is approximately 44,96,694.

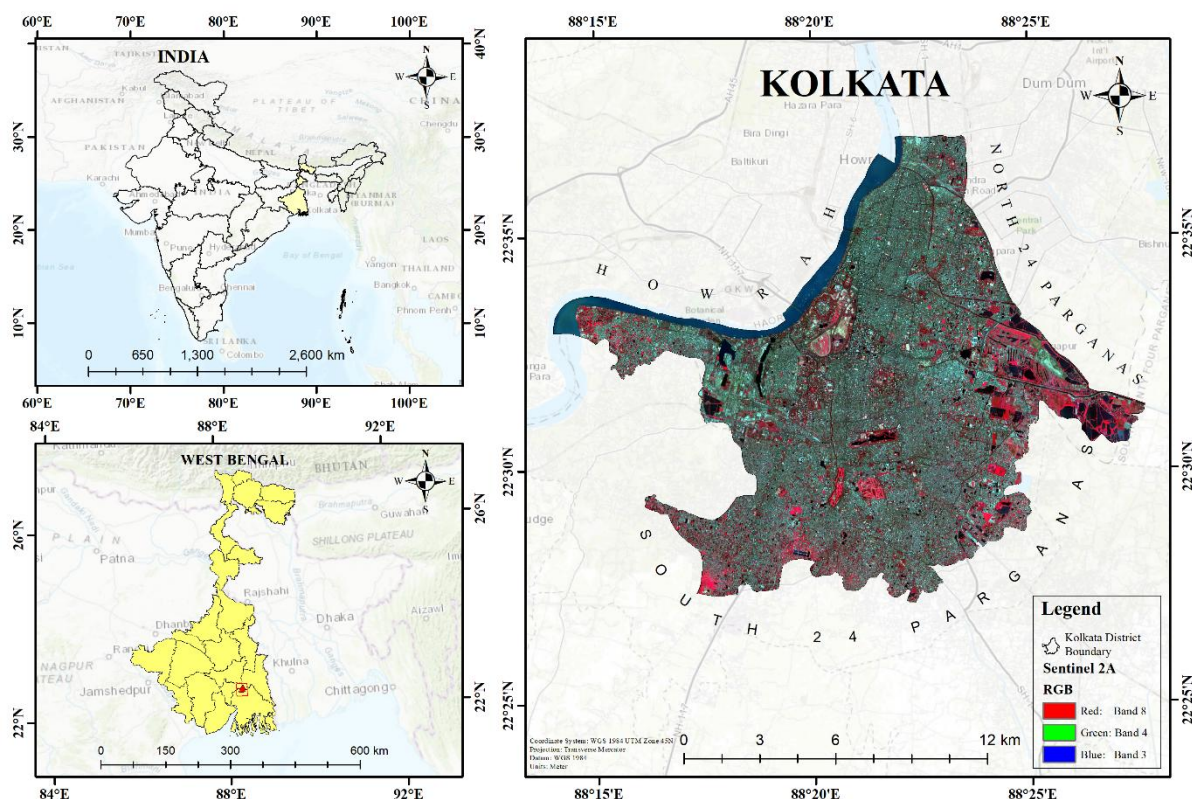


Figure 3.1: Location map of the study area

3.1 Physical Characteristics of the study area

3.1.1 Topography:

The soil, on which the Kolkata district is built, happens to be a part of the alluvial deposit of the Gangetic delta and the elevation is not more than 5 to 6 meters. The texture of the soil varies from sandy loam to clay loam.

The principal river of the district is the Ganges (Hooghly). The most important tributary of the Hooghly is the Bhagirathi. The width of the river Hooghly varies from 55 meters to 2.4 Km. The maximum height of the district above sea level is 5.3 meters.

Chapter -3: Description of the Study area

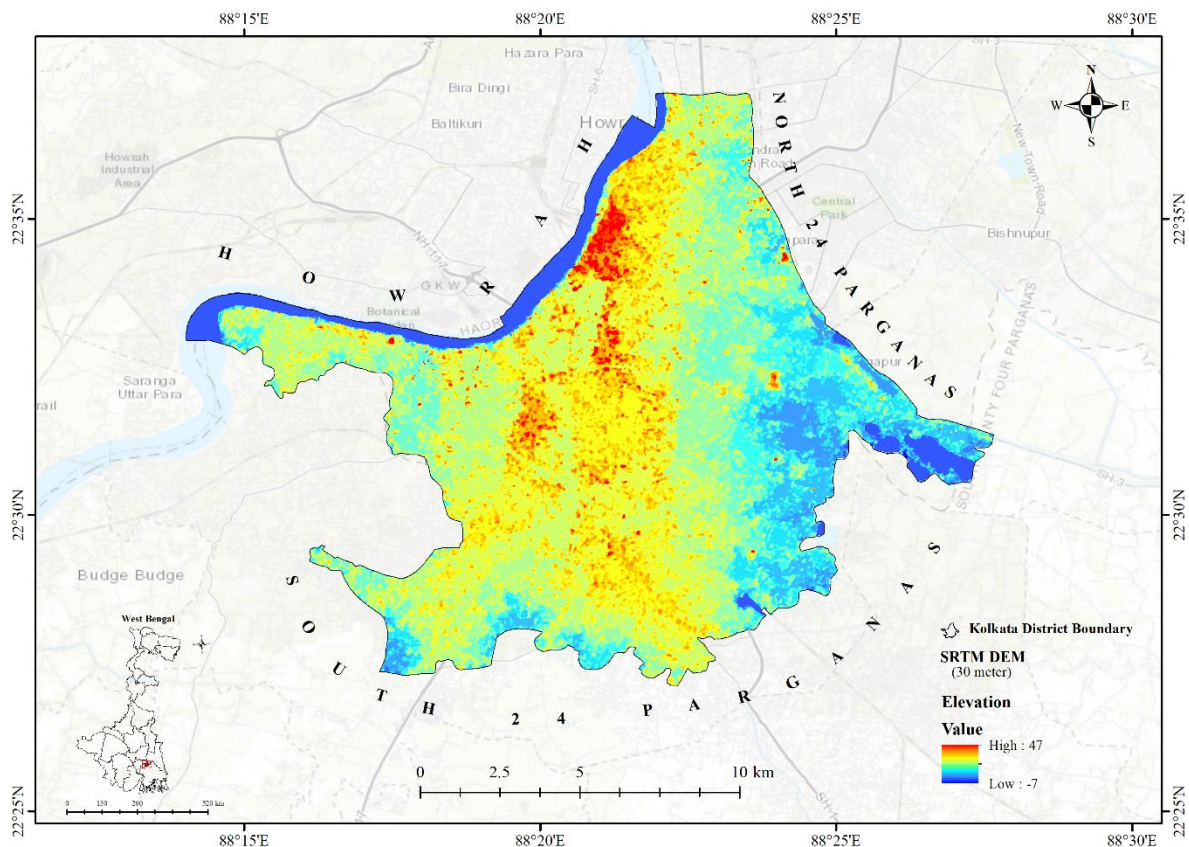


Figure 3.2: Elevation map of Kolkata district

Source: Prepared in ArcGIS

3.1.2 Climate of Kolkata:

Kolkata has a tropical wet-and-dry climate with three main seasons—summer, monsoon, and winter. The summer season lasts from March to June; it is hot and humid with temperatures rising to around 35°C (95°F) and humidity as high as 90 percent. The monsoon season, which lasts from June to September, brings tropical rains to the city; average annual rainfall is about 1,800 mm and the city is often flooded. From December to February, the winter season, temperatures range comfortably from 12°C (54°F) to 25°C (77°F). ([https://en.wikipedia.org/wiki/Geography_of_Kolkata_\(2024\)](https://en.wikipedia.org/wiki/Geography_of_Kolkata_(2024)))

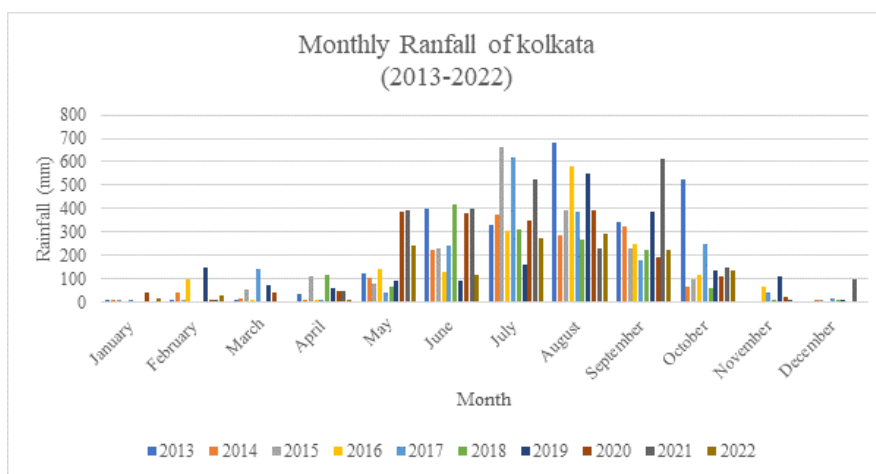
Year	Jan	Feb	M	April	May	June	July	Aug	Sept	Oct	Nov	Dec	Total Rainfall (mm)
2013	12.2	9.9	1.2	31.2	122.4	397.5	327.5	679.2	341.4	523.1	0	0	2445.6
2014	1	41.5	16.3	0.1	101.4	223.5	376	283.6	322.1	65.5	0	0.1	1431.1
2015	3.2	6.8	53.5	112	78.9	226.2	663.8	389.9	229.3	98.5	0	3.2	1865.3
2016	0	94.5	8.9	0.2	141	131.2	301.3	583.8	246	117	65.5	0	1689.4
2017	0.1	0	138.9	4.5	41.9	240	621.5	385.9	181.9	247.2	41.7	16.7	1920.3
2018	0	0	0	113.7	64	419.7	307.9	268.7	221.5	56.6	5.6	9.3	1467

Chapter -3: Description of the Study area

2019	0	147.2	69.6	60.1	90.5	91.5	159.9	548.6	387	137.6	111.4	11.8	1815.2
2020	42.5	3.5	39.4	49	383.7	381.9	348.2	389.7	189.1	107	24	0	1958
2021	0	1.5	0	44.7	391.4	401.8	525.2	229	613.8	144.3	2.1	97.7	2451.5
2022	13	30.8	0	0.2	242.3	115.8	275.2	291	223.5	133.3	0	0	1325.1

Table 3: Monthly rainfall of Kolkata district from 2013 to 2022 (last 10 years)

Source: Hydro IMD



Graph 1: Last 10 years rainfall data graph

Source: Hydro IMD

3.1.3 Geology and Geomorphology of Kolkata:

Kolkata is situated on the Bengal Basin, which is one of the world's largest sedimentary basin. It is a pericratonic tertiary basin made up of three structural units, the shelf or platform in the west, the central hinge or shelf/slope break, and the deep basinal part in the east and the southeast (Bose et al., 2020). The western part of the hinge zone on which the city of Kolkata is located is about 25 km wide and approximately 45,000 meters thick with sediments dipping about 7,500 meters below the present surface. In the recent or latest Pleistocene to Holocene period, the Quaternary sediments of the Bengal Basin occupy the top 350-450 meters. The Tertiary, Cretaceous trap wash and the Permian-Carboniferous Gondwana rocks follow this. Kolkata is located in the boundary between seismic zone III and zone IV which denotes a moderate earthquake-prone area (Walling & Mohanty, 2009).

https://en.wikipedia.org/wiki/Geography_of_Kolkata

Chapter -3: Description of the Study area

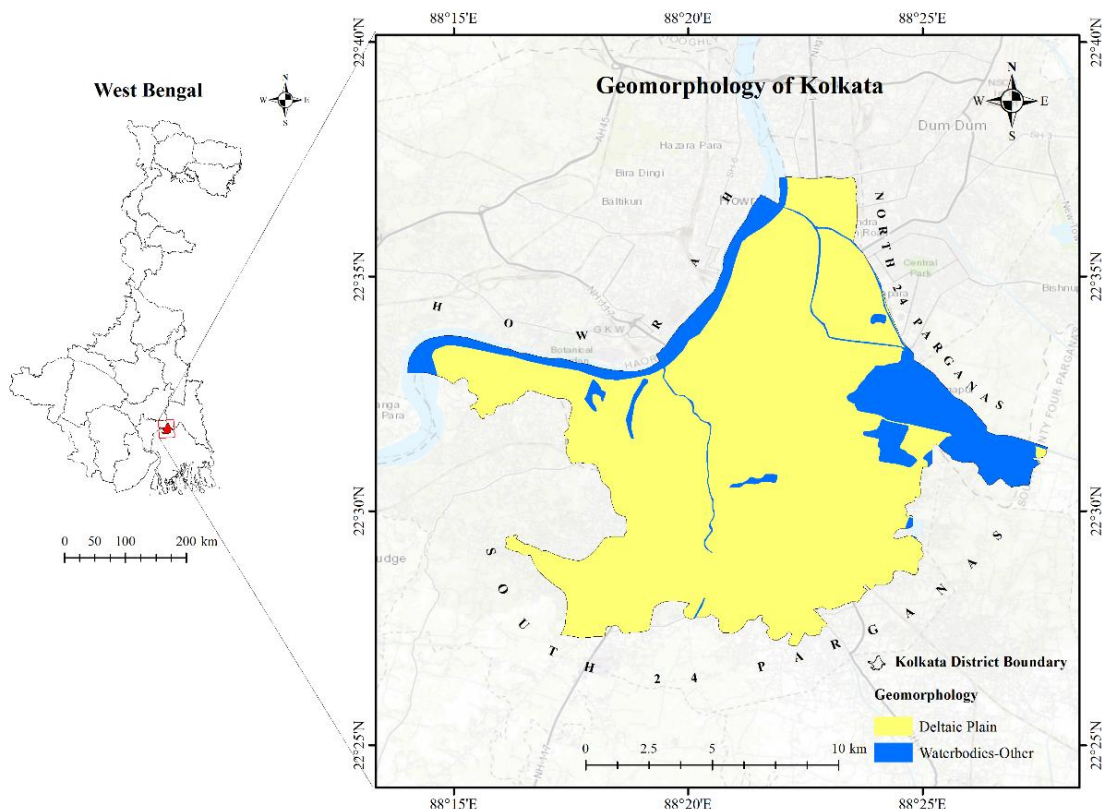


Figure 3.3: Geomorphology of Kolkata district

Source: Prepared in ArcGIS

3.1.4 Lithology:

The Archean crystalline rocks occur as basement, overlaid by Tertiary formation, and Quaternary sediments consist of fine to coarse grains of sand, silt, and clay. The top 3 m from the ground surface contains a mixture of sand and silty clay; followed by a thick layer of clay that ranges up to a depth ranging from 15 m to 50 m. The clay with an average thickness of 40 m occurs on the upper part of the sedimentary sequence. This clay formation functions as a confining layer. Beyond this, a sandy formation containing fine, medium, and coarse sand and pebbles occurs up to a depth of about 300 m. The sand formation functions as a confined aquifer. A thick surface of clay layer at the top of the sedimentary sequence in the surface restricts the rainfall recharge. The recharge area of this confined aquifer is located at a distance of about 65 km north of Kolkata, and most of the recharge occurs from August to October (Chatterjee et al., 2006). The lithology map of Kolkata is shown in Figure 3.4

Chapter -3: Description of the Study area

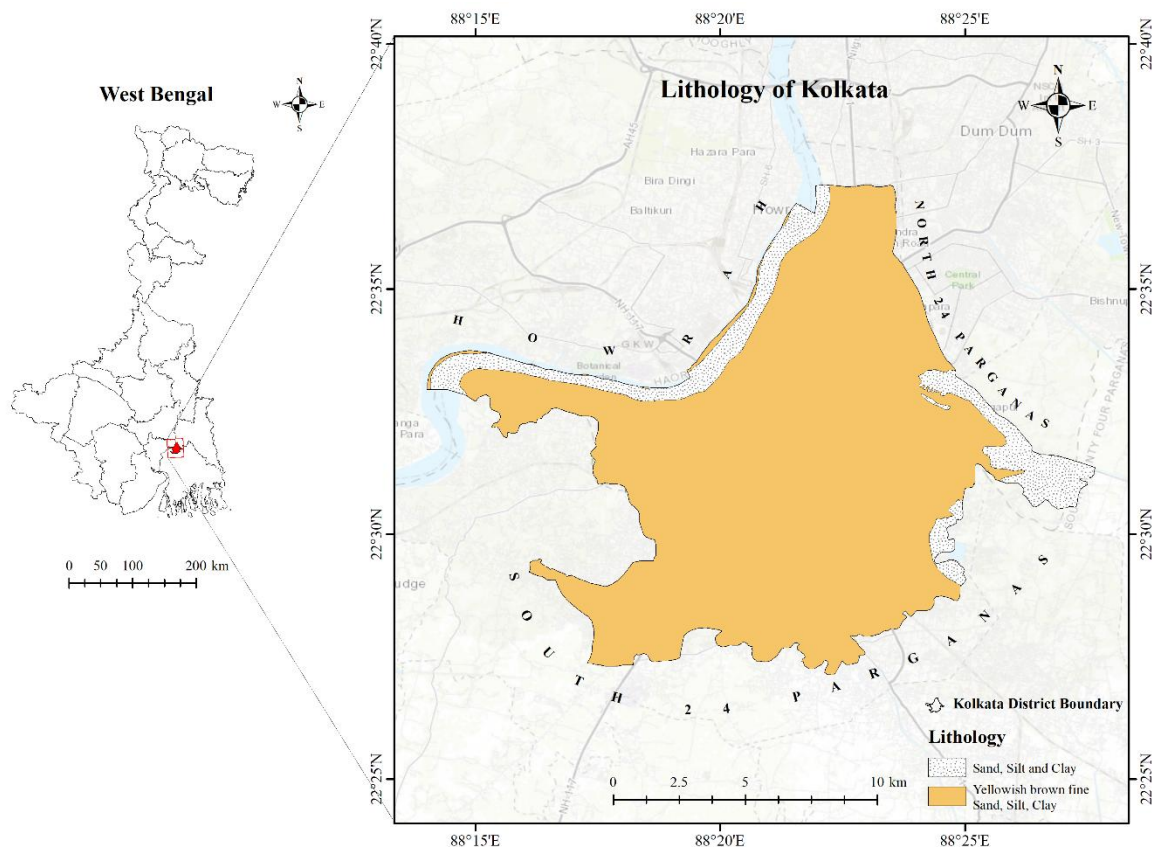


Figure 3.4: Lithology of Kolkata district

Source: Prepared in ArcGIS

3.2 Socio-economic characteristics:

3.2.1 Population:

Kolkata is the only district in West Bengal State which is entirely urbanized. According to Census 2011, Population of the Kolkata city is 44,96, 694. Where the male population is 23,56,766 and the female population is 21,39, 928. Kolkata district ranks 10th position in terms of total population. Kolkata has the lowest scheduled tribe and scheduled caste population in the state. The density of Kolkata district is 24,306 people per square km. Kolkata is the 2nd most literate (86.3%) district of West Bengal. where the male literacy rate is 88.34% and the female literacy rate is 84.06%. The sex ratio of the Kolkata district is 908 females per 1000 males.

3.2.2 Transport and Communication:

Kolkata has an extensive network of transportation and communication. The road transportation options in the city include a vast bus network, iconic yellow cabs, autorickshaws, and app-based ride-sharing services such as Uber and Ola. Metro transport is also present, Kolkata Metro is the oldest in India. The railway network connected Kolkata to other cities in India. Netaji Subhas Chandra Bose International Airport connects Kolkata with different cities of the world. Ferries on the Hooghly River and Kolkata Port, a significant riverine port, are examples of water transportation. The city also has robust telecommunications and internet services, provided by major operators such as BSNL, Airtel, Vodafone Idea, and Jio, alongside a wide postal network. To improve urban infrastructure, recent advancements have concentrated on growing metro lines and smart city projects.

Chapter – 4

Data and Methodology

4 Materials and methods:

The study utilized various types of satellite imagery such as Sentinel-1A and Sentinel-2A to create a map of the study area. In addition, the study used SRTM DEM to align the Sentinel-1A images. To process the data, this study also used different open-source software packages like snap2stamps, StaMPS master, and TRAIN. All of these software programs and open-source packages are installed on the Linux Operating System, as StaMPS master is most suitable for Linux. This study also used the Matlab software to process the data through the StaMPS master.

4.1 Materials

4.1.1 Sentinel-1 SLC Data:

Sentinel-1lun Sentinel-1A, a C-band SAR satellite, was launched by ESA on April 3, 2014. It is in a sun-synchronous, near-polar, circular orbit with a 693 km orbit height, 98.18° inclination, and a 12-day repeat cycle at the equator.

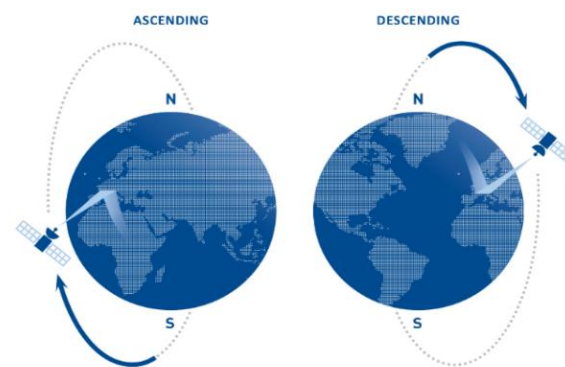


Figure 4.1: Ascending and Descending orbit of Sentinel-1 SAR images

Source: Tre Altamira

All SAR satellites travel from the north pole towards the south pole for half their trajectory. This direction is referred to as their descending orbit. Conversely, when satellites travel from the south towards the north pole, it is said to be in an ascending orbit. The same area is revisited along the two orbits (shown in Figure 4.1). Consequently, ascending and descending imageries are collected over the same location.

We need a minimum of 20 to 25 images to analyze land subsidence using PSInSAR. If you need to download multiple images, you can follow this shortcut process on the ASF website:

To begin, open the terminal on your device and enter the command "`pip install aria2c`" to install the aria2c tool. This Python library allows you to download multiple images from ASF. Next, go to the ASF data search, look for the data you need (e.g., I selected the Kolkata region and chose Sentinel-1 SLC data with an ascending flight direction), and add it to your cart. Once you have added the data to your cart, download the Metalink file to proceed with the download process.

Chapter -4: Data and Methodology

Go to the folder where you need to download the file. Open terminal in this folder and type
`aria2c --http-user='<username>' --http-passwd='<password>' --check-certificate=false -M <file_name>.metalink`

<username>: Your ASF login username

<passwd>: Your ASF login password

<file_name>: Enter your download metalink file name

In this process, you will download multiple images from the ASF website.

4.1.2 Sentinel 2A data:

Sentinel-2A was launched on 23 June 2015 as part of the European Space Agency's Copernicus program for land monitoring using high-resolution optical images. It operates in a sun-synchronous orbit at an altitude of 786 km, which allows it to revisit the same area every 5 days. The satellite's Multispectral Instrument (MSI) captures imagery across 13 spectral bands, with spatial resolutions of 10 m, 20 m, and 60 m, and a swath width of 290 km. This makes Sentinel-2A very useful for land cover classification, agricultural monitoring, forestry management, disaster control, coastal monitoring, extracting further information in water bodies, and urban planning. Therefore, Sentinel-2A is an essential tool for environmental monitoring and management. All the description about the band of sentinel 2A image are in Table 12.

From this sentinel 2A image, Band 8, Band 4, and Band 3 is used for creating Study area map of the Kolkata district.

Sentinel-2A Bands	Central Wavelength (nm)	Bandwidth (nm)	Spatial Resolution (m)
Band 1 – Coastal aerosol	442.7	21	60
Band 2 – Blue	492.4	66	10
Band 3 – Green	559.8	36	10
Band 4 – Red	664.6	31	10
Band 5 – Vegetation red edge	704.1	15	20
Band 6 – Vegetation red edge	740.5	15	20
Band 7 – Vegetation red edge	782.8	20	20
Band 8 – NIR	832.8	106	10
Band 8A – Narrow NIR	864.7	21	20
Band 9 – Water vapour	945.1	20	60
Band 10 – SWIR – Cirrus	1373.5	31	60
Band 11 – SWIR	1613.7	91	20
Band 12 – SWIR	2202.4	175	20

Table 4: Sentinel 2A satellite Bands with their central wavelength and Spatial resolution

Source: ESA

4.1.3 SRTM data:

The Shuttle Radar Topography Mission (SRTM) which was launched by NASA on February 11 2000 marked a milestone in obtaining digital elevation information, about the Earth's surface. Positioned in an orbit at an altitude of 233 km with a 57-degree inclination SRTM used two radar antennas. C band and X band Synthetic Aperture Radar. To map approximately 80% of the Earths land area between 60 degrees North and 56 degrees South latitude. The mission

Chapter -4: Data and Methodology

achieved a resolution of 30 meters for the United States and 90 meters globally using C band data while X band data provided resolution but limited coverage. SRTMs horizontal accuracy was 20 meters. Vertical accuracy is around 16 meters. The data processed through Interferometric Synthetic Aperture Radar (InSAR) has played a role in fields such, as topographic mapping, hydrology, geology, environmental research, infrastructure development planning, and disaster response. This has led to the creation of a comprehensive digital topographic database of Earth's surface to date.

This SRTM DEM is used to co-register the sentinel 1 SLC master and slaves images.

4.1.4 Opensource software packages:

ESA SNAP software and various open-source packages such as snap2stamps, StaMPS, SNAPHU, TRAIN, and Triangle-bin are employed for Sentinel-1 SLC data processing.

SNAP stands for Sentinel Application Platform which is an open-source software to process all types of sentinel datasets. To download this software, go through this link <https://step.esa.int/main/download/snap-download/>.

Snap2Stamp is a tool that automatically pre-processes Sentinel-1 SLC data using the SNAP GPT (Graph Building Tools). To download this package, go through this link <https://github.com/mdelgadoblasco/snap2stamps>.

StaMPS (Stanford Method for Persistent Scatterers) is a technique for the analysis of Synthetic Aperture Radar (SAR) data that allows for the detection and measurement of ground deformation by analyzing the phase information of the radar signals. It is a popular software package used for processing Sentinel-1 and other SAR data for various applications such as land subsidence monitoring, volcano monitoring, and earthquake analysis. To download the software package, go through this link <https://github.com/dbekaert/StaMPS>.

SNAPHU stands for Statistical-Cost, Network-Flow Algorithm for Phase Unwrapping which was developed by Stanford Radar Interferometry Research Group. It is a tool designed for two-dimensional phase unwrapping. This process involves recovering unambiguous phase data from a 2-D array of phase values known only modulo 2pi rad. SNAPHU attempts to compute congruent phase-unwrapped solutions that are maximally probable in an approximate a posteriori sense. The algorithm's solver routine is based on network optimization. It is commonly used in synthetic aperture radar (SAR) interferometry. To Download this package, go through this link <https://web.stanford.edu/group/radar/softwareandlinks/sw/snaphu/>.

TRAIN (Toolbox for Reducing Atmospheric InSAR Noise) is a toolbox used to remove atmospheric noise from InSAR images. To download this toolbox, go through this link <https://github.com/dbekaert/TRAIN>.

4.1.5 Matlab software:

In the time of installing Matlab software, we need the specific packages like:

- Curve Fitting Toolbox
- Financial Toolbox
- Image Processing Toolbox
- Mapping Toolbox
- Optimization Toolbox
- Parallel Computing Toolbox
- Signal Processing Toolbox
- Statistics and Machine Learning Toolbox

4.2 Methodology

4.2.1 Data pre-processing:

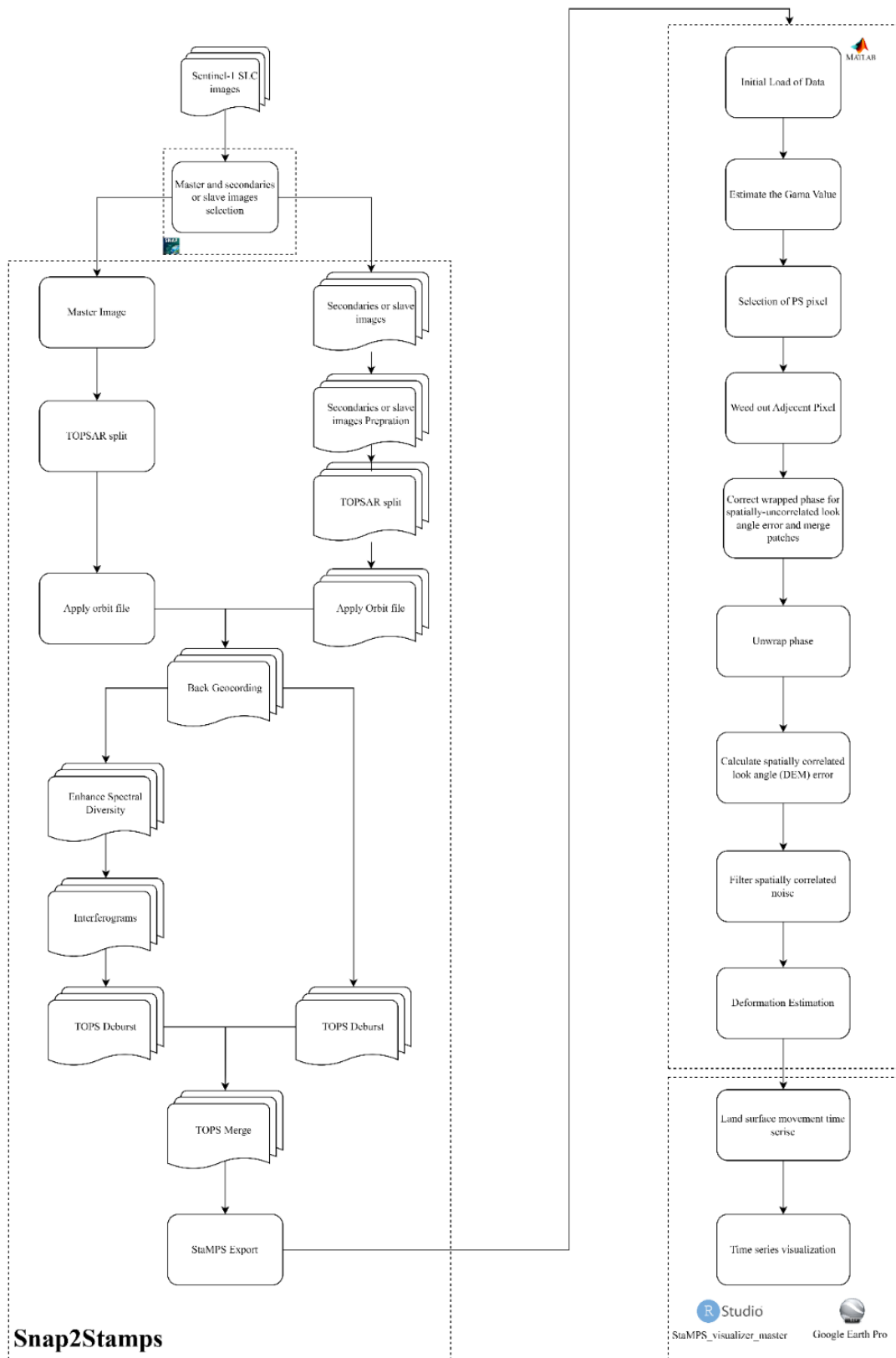


Figure 4.2: Methodological Workflow for PSInSAR integration with StaMPS

Chapter -4: Data and Methodology

After downloading all 21 Sentinel-1 SLC images from the Alaska Satellite Facility (ASF: <https://search.asf.alaska.edu/#/>). Separated the total data into Master and Slave images for Land Subsidence monitoring.

The pre-processing starts with selecting the Master image, which is used as a reference for processing all the secondary or slave images.

To choose the Master image, open the SNAP software and add all the data. Then, navigate to Radar → Interferometric → Stack Overview → select Optimal InSAR Reference Selection. Input all the images, and the SNAP software will select the master image and secondaries or slave images for you.

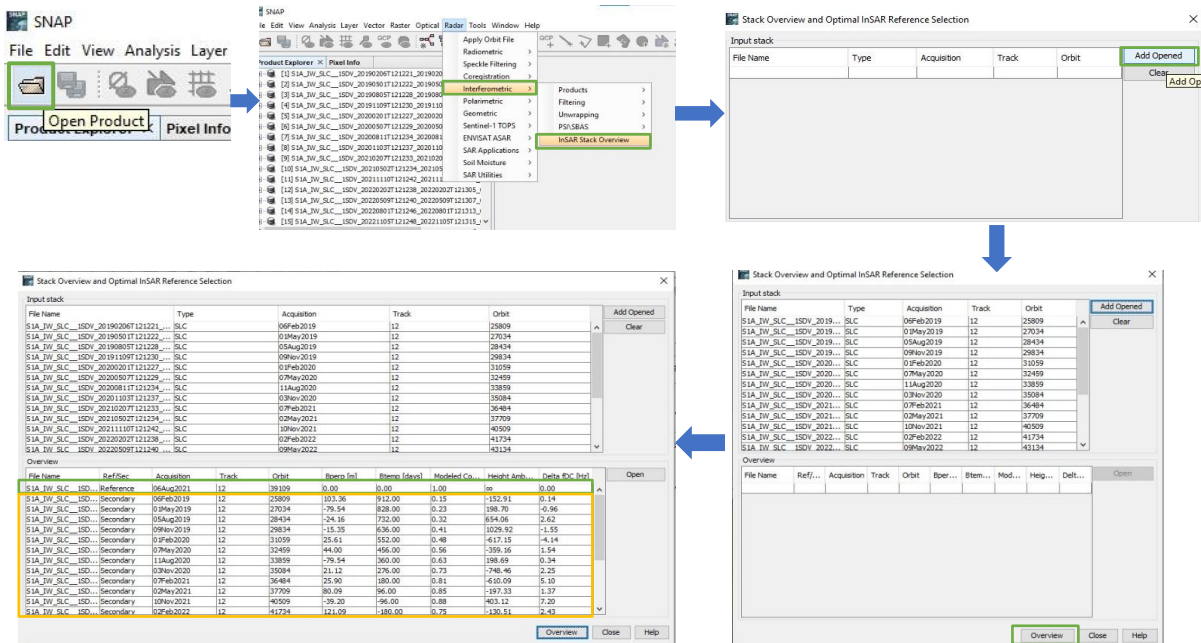


Figure 4.3: Process of Finding Master and Slaves or Secondary Images

Master or slave images	Path	Frame	flight directions	Polarization	Acquisition Date	Perpendicular Baseline (m)	Temporal baseline (m)
Master Image	12	69	Ascending	VV	2021-08-06	0	0
Slave image	12	69	Ascending	VV	2024-02-04	28	912
Slave image	12	69	Ascending	VV	2023-11-12	40	828
Slave image	12	69	Ascending	VV	2023-08-08	91	732
Slave image	12	69	Ascending	VV	2023-05-04	-21	636
Slave image	12	69	Ascending	VV	2023-02-09	136	552
Slave image	12	69	Ascending	VV	2022-11-05	79	456

Chapter -4: Data and Methodology

Slave image	12	69	Ascending	VV	2022-08-01	-31	360
Slave image	12	69	Ascending	VV	2022-05-09	12	276
Slave image	12	69	Ascending	VV	2022-02-02	120	180
Slave image	12	69	Ascending	VV	2021-11-10	-37	96
Slave image	12	69	Ascending	VV	2021-05-02	78	-96
Slave image	12	69	Ascending	VV	2021-02-07	20	-180
Slave image	12	69	Ascending	VV	2020-11-03	17	-276
Slave image	12	69	Ascending	VV	2020-08-11	-81	-360
Slave image	12	69	Ascending	VV	2020-05-07	43	-456
Slave image	12	69	Ascending	VV	2020-02-01	16	-552
Slave image	12	69	Ascending	VV	2019-11-09	-9	-636
Slave image	12	69	Ascending	VV	2019-08-05	-25	-732
Slave image	12	69	Ascending	VV	2019-05-01	-82	-828
Slave image	12	69	Ascending	VV	2019-02-06	102	-912

Table 5: Master and Slaves or Secondary image with their Acquisition date, Temporal Baseline, Perpendicular Baseline

Through this process, the Master image is identified as August 6th, 2021, while all other images were secondary or slave images. It shown in the Figure 4.4.

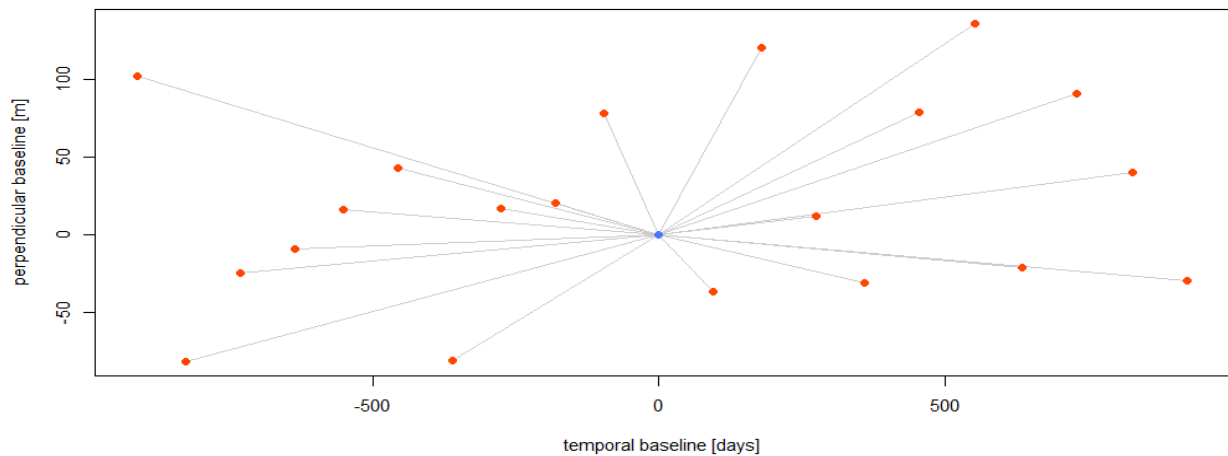


Figure 4.4: Image acquisition graph with their Perpendicular and Temporal Baseline

Source: created in Stamps-visualizer

After finding the master image the study needs to prepare this image through snap2stamps scripts.

Snap2Stamps software package has a configuration file called Project_topsar.conf which specifies the input and output paths for your data, the location of the master data path, and an Area of Interest (AOI) to split the IW sub-swath of master and slave images.

Chapter -4: Data and Methodology

```
1 ##### TOPSAR CONFIGURATION FILE #####
2
3 [PROJECT_DEFINITION]
4 PROJECTFOLDER = G:/Data and processing/Project
5 PROJECTNAME = Project
6
7 [[PROC_OPTIONS]]
8 N_OPTIONS =
9 OVERWRITE = N
10 SMARTDD = N
11 PLOTTING = Y
12
13 [[PARAMETERS]]
14 SENSOR = S1
15 SENSOR = S1
16 POLARISATION = VV
17 MASTERSOURCE = G:/Data and processing/Original/MASTER
18 # MASTER_SEL : AUTO / FIRST / LAST / MANUAL
19 #MASTERSEL = MANUAL
20 EXTEND =
21
22 [[AOI_DEFINITION]]
23 #AOI_MODE OPTIONS WKT / BBOX / SHP / KML / GeoJSON
24 AOI_MODE = WKT
25 #AOI_WKT =
26 #LATMIN = 51.20
27 #LONMAX = 7.57
28 #LATMAX = 51.20
29 #LONMIN = 7.57
30 #AOI_FILE = /tmp/my.aoi.shp
31
32 [[SEARCH_PARAMS]]
33 autoDownload = Y / N
34 autoDownload = N
35 TRACK = 95
36 beamMode : SLC / GRD
37 beamMode = SLC
38 START / STOP in YYYY-MM-DD
39 START = 2022-01-01
40 END = 2022-04-15
41 # SAT : S1 / S1A / S1B
42 SAT = S1A
43 ASF_USER =
44 ASF_PASS =
45 # Number of Parallel Downloads (NPD)
46 SEARCH_PDOWNLOADS =
47 NPD = 4
48
49 [[SNAP_GPT]]
50 SNAP_INSTALLATION_FOLDER = C:/Program Files/snap
51 SNAP_HOME_DIR = C:/Program Files/snap
52
53 [[COMPUTING_RESOURCES]]
54 CPU = 4
55 CACHE = 12G
56
```

In order to prepare the master and secondary images for StaMPS PSI processing, open the Snap2Stamps configuration file named "project_topsar.conf". From there, need to some changes to the input path, export path, path of the master data, and the AOI data. The AOI can be input as either a BBOX or SHP file format or as maximum and minimum latitude and longitude information. In addition, the study also needs to configure the SNAP GPT path and computing resource power, such as the core count of your CPU and free RAM, according to the computer.

4.2.2 Data processing:

This study's workflow for detecting land subsidence has been divided into two parts.

1. Data pre-processing with Snap2stamps
2. Data processing through StaMPS in Matlab

4.2.2.1 Data pre-processing with snap2stamps

After configuring the Project_topsar.conf file there are several steps for processing sentinel-1 SLC images for StaMPS. In the latest version of snap2stamps, all the processes are automatically executed from data download to StaMPS export. However, this study adopts a step-by-step process to understand the entire process better. This involved data downloading, selection of master and secondary or slave images, slave preparation, master image splitting, slave images splitting, co-registrations, interferograms generation, and StaMPS export.

Name	Date modified	Type	Size
asf_s1_downloader.py	12-01-2024 19:00	PyCharmCE2023.3	4 KB
auto_run.py	12-01-2024 19:00	PyCharmCE2023.3	4 KB
project_stripmap.conf	12-01-2024 19:00	CONF File	2 KB
project_topsar.conf	21-04-2024 16:09	CONF File	2 KB
stripmap_step_0a_unpack_sar_scenes.py	12-01-2024 19:00	PyCharmCE2023.3	4 KB
stripmap_step_0b_secondaries_prep.py	12-01-2024 19:00	PyCharmCE2023.3	3 KB
stripmap_step_1_subset_sar.py	12-01-2024 19:00	PyCharmCE2023.3	7 KB
stripmap_step_1b_masterselection.py	12-01-2024 19:00	PyCharmCE2023.3	3 KB
stripmap_step_2_coreg_sar.py	12-01-2024 19:00	PyCharmCE2023.3	6 KB
stripmap_step_3_ifg_sar.py	12-01-2024 19:00	PyCharmCE2023.3	6 KB
stripmap_step_4_plotting_all.py	12-01-2024 19:00	PyCharmCE2023.3	20 KB
stripmap_step_5_stamps_export.py	12-01-2024 19:00	PyCharmCE2023.3	6 KB
topsar_automaster.py	12-01-2024 19:00	PyCharmCE2023.3	3 KB
topsar_step_0_secondaries_prep.py	12-01-2024 19:00	PyCharmCE2023.3	3 KB
topsar_step_1_splitting_master_multi_IW...	12-01-2024 19:00	PyCharmCE2023.3	8 KB
topsar_step_2_splitting_secondaries.py	12-01-2024 19:00	PyCharmCE2023.3	9 KB
topsar_step_3_coreg_ifg_topsar_smart.py	12-01-2024 19:00	PyCharmCE2023.3	11 KB
topsar_step_4_plotting_all.py	12-01-2024 19:00	PyCharmCE2023.3	8 KB
topsar_step_5_stamps_export_multilW.py	12-01-2024 19:00	PyCharmCE2023.3	9 KB

Configure file

Sentinel-1 SLC processing Python file

4.2.2.1.1 Secondaries or slave images preparation:

In this step, sentinel-1 SLC secondary or images are shorted by acquisition date. To run this step, go to your device terminal and type [python topsar_step_0_secondaries_prep.py -

Chapter -4: Data and Methodology

[F project_topasar.conf] and then press enter. In this way, secondaries or slave images are sorted according to the Acquisition date.

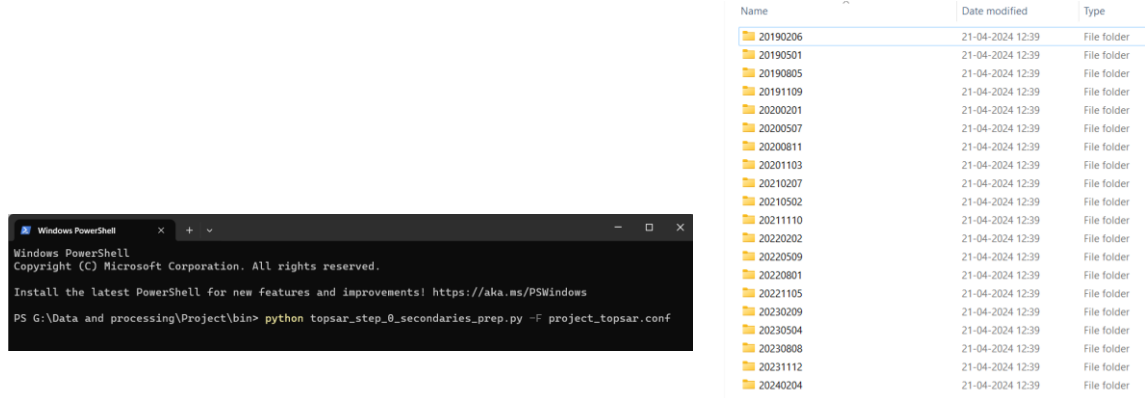
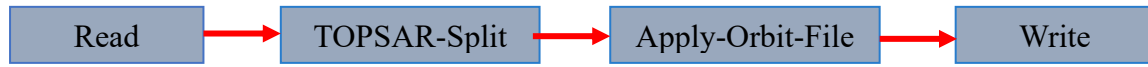


Figure 4.5: Shorting and storing the Secondaries or Slaves image according to the dater

4.2.2.1.2 Master image preparation:

The second step is master image preparation using the snap2stamps Python scrip. This involves splitting the master image based on the study boundary and applying the orbit file, which can be downloaded through ESA SNAP GPT. The preparation of the master image is carried out through this graph.



graph 2: Master Image Splitting Graph

To run this step, go to the bin folder of your snap2stamps then open the terminal in this bin folder, and type [python topsar_step_1_splitting_master_multi_IW.py -F project_topasar.conf] then press enter.

In this master image, the study boundary lies on IW1(Interferometric Wide swath) and IW2 (Interferometric Wide swath) that shows in Figure 4.6.

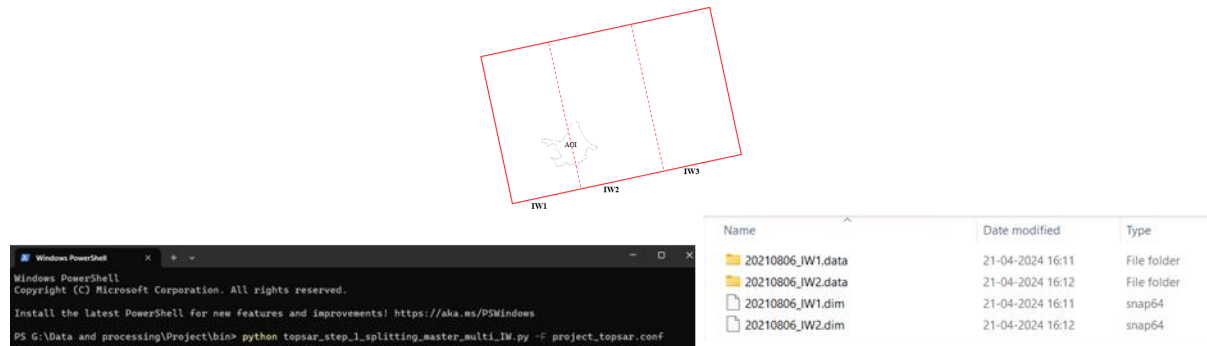
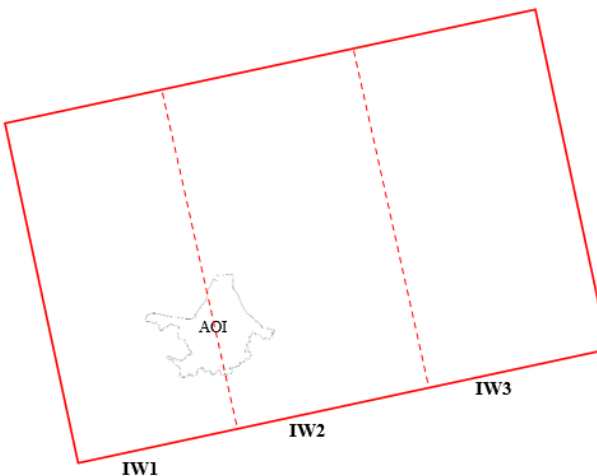


Figure 4.6: Sentinel 1 SLC image IW (Interferometric Wide) swath graph and 2 IW swath created by the Master Image splitting graph.

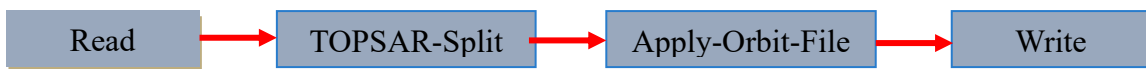
4.2.2.1.3 Splitting the secondaries or slave images:

The process of splitting secondaries is similar to that of splitting the master image. To split secondaries or slave images go to the bin folder of your snap2stamps and then open the terminal in the bin folder and type [python topsar_step_2_splitting_secondaries.py -F project_topasar.conf] then press enter.



The study area lies between IW1 and IW2 sub-swath that shows above. The preparation of the secondaries or slave images is carried out through this graph 3.

All the secondaries or slave images are split into IW1 and IW2 as the master image split.



graph 3: Secondaries or Slave Image splitting processing graph

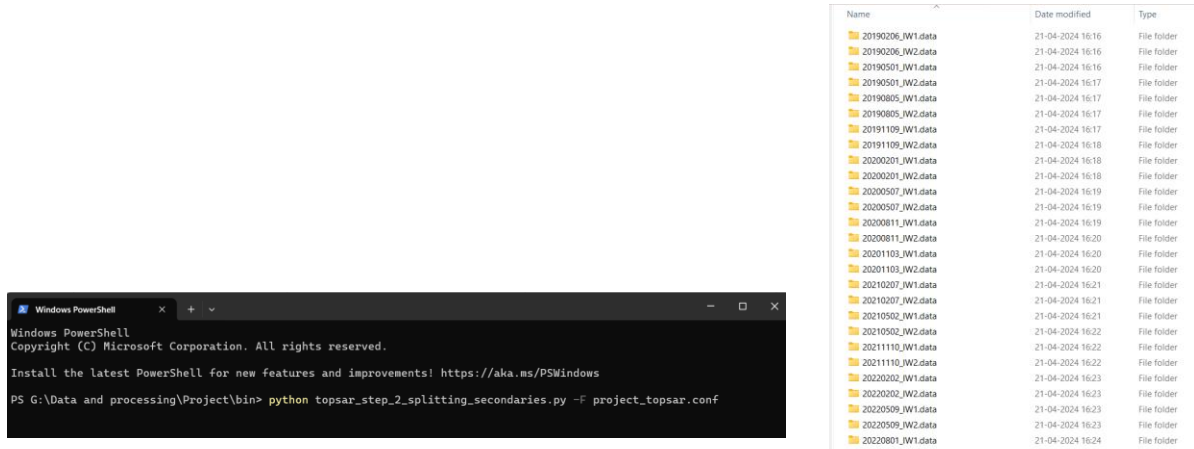
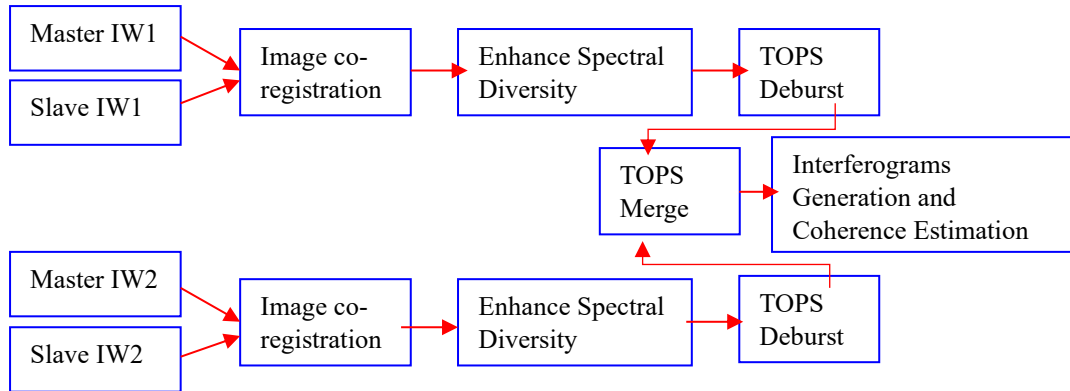


Figure 4.7: All Slaves images split through graph 3 in Snap2stamps

4.2.2.1.4 Coregistration and interferogram generation:

When working with multiple images, it's crucial to ensure that they are correctly aligned with a reference image. This process is known as image coregistration and can be achieved using the S-1 Back Geocoding operator. To perform this process successfully, we need a Digital Elevation Model (DEM), which can be downloaded from SNAP. We used the SRTM 1arc second DEM, but other external high-resolution DEMs can also be used. The DEM provides accurate coordinate information necessary for the image coregistration process.

Chapter -4: Data and Methodology



graph 4: Coregistration and interferogram generation methodology graph

Once the coregistration process is complete, Enhanced Spectral Diversity (ESD) can be used. ESD is a technique used in Persistent Scatterer Interferometry (PSInSAR) to improve the accuracy of interferograms, especially for Terrain Observation with Progressive Scans (TOPS) mode data acquired by satellites like Sentinel-1.

Radar images are captured in rapid bursts, rather than a single continuous scan. This allows for faster data acquisition but also introduces slight shifts between these bursts. These shifts can cause phase discontinuities at the boundaries between bursts in the interferogram. The TOPS Deburst process aims to remove these phase discontinuities by estimating and correcting for the misalignment between bursts. This correction typically involves calculating a constant azimuth shift to align the bursts within the interferogram. By mitigating these discontinuities, TOPS Deburst improves the accuracy and reliability of PSInSAR measurements.

After TOPS Deburst, we need to merge the two TOPS Deburst data since our study area is in the two IW (Interferometric Wide swath).

Interferogram generation and coherence estimation are essential steps in Persistent Scatterer Interferometry (PSInSAR) used to measure ground deformation. An interferogram is produced by combining two Synthetic Aperture Radar (SAR) images of the same area acquired at different times. Each SAR image captures the phase information of reflected radar signals. Subtracting the phase information of corresponding pixels in the two images generates an interferogram. The resulting values in the interferogram represent the phase difference between the two acquisitions, which can be related to surface displacement or other changes.

Coherence is a measure of the similarity between the two SAR images used to generate the interferogram. Ideally, the images should be highly similar for accurate phase difference measurements. Factors like changes in ground cover, vegetation growth, or the presence of moving objects can reduce coherence and introduce noise into the interferogram. Coherence estimation calculates a value between 0 (no similarity) and 1 (perfect similarity) for each pixel in the interferogram. Pixels with high coherence values are considered more reliable for PSInSAR analysis, as they represent a stronger signal and less noise.

To process step 4 go to the bin folder of snap2stamps and open the terminal then type [`python topsar_step_3_coreg_ifg_topasar_smart.py -F project_topasar.conf`] and then press enter.

4.2.2.1.5 StaMPS Export:

The final step of snap2stamp is to export the interferograms for StaMPS processing. To run step 5 go to the bin folder of snap2stamps and open the terminal then type [python topsar_step_5_stamps_export_multiIW.py -F project_topsar.conf] and then press enter.

Name	Date modified	Type
bin	12-01-2024 19:00	File folder
coreg	21-04-2024 16:29	File folder
graphs	12-01-2024 19:00	File folder
ifg	21-04-2024 16:29	File folder
INSAR_20210806	21-04-2024 18:11	File folder
logs	21-04-2024 16:11	File folder
MasterSplit	21-04-2024 16:11	File folder
secondaries	21-04-2024 12:19	File folder
split	21-04-2024 16:16	File folder

Name	Date modified	Type
dem	21-04-2024 18:11	File folder
difff	21-04-2024 18:11	File folder
geo	21-04-2024 18:11	File folder
rslc	21-04-2024 18:11	File folder

Figure 4.8: StaMPS exported file screenshot which is used in the PSInSAR process

4.2.2.2 Data processing through StaMPS in Matlab

After StaMPS export there is an INSAR_20210806 folder generated. The study need to prepare the file for StaMPS processing. To do that install the StaMPS master software package properly. Then go to the INSAR_20210806 folder open the CMD and type `mt_prep_snap20210806/home/amit/Documents/Land_subsidance_2019_2024/INSAR_20210806 0.4 1 1 50 50` and then hit enter.(Hooper et al., 2018)

Here's what each parameters means:

`mt_prep_snap` is the command that is used to process the data through SNAP

`20210806` = It is the master date.

`/home/amit/Documents/Land_subsidance_2019_2024/INSAR_20210806` = StaMPS export folder path,

`0.4` refers to the Amplitude dispersion (0.4-0.42 is a reasonable value),

`1` refers to the number of patches in the range direction (here I used the default value, 1),

`1` refers to the number of patches in the azimuth direction (here I used the default value, 1),

`50` refers to overlapping pixels between patches in range (default 50),

`50` refers to overlapping pixels between patches in azimuth (default 50),

The number of patches depends on the study area's size and the computer's processing power.(Hooper et al., 2018)

Amplitude Dispersion Index (ADI) is amplitude standard deviation divided by mean amplitude. This means a pixel that has a constant value over the entire period (e.g. a building or bare soil) has a low standard deviation and therefore a small dispersion. If it changes its backscatter intensity over time (e.g. agriculture, water, forest), the standard deviation is high which makes the dispersion large. This is very important to select PS points from the SAR images. The Amplitude Dispersion Index (ADI) calculated by this

$$ADI = \frac{\sigma_A}{m_A}$$

Chapter -4: Data and Methodology

σ_A is the standard deviation of amplitude of the RADAR signal over time, m_A is the mean amplitude of the RADAR signal over time.

Amplitude dispersion is used to calculate indicators for the stability of a pixel over time called as Amplitude Stability Index.

The Amplitude Stability Index (ASI) was calculated by this 5.

$$ASI = 1 - \frac{\sigma_A}{m_A}$$

4

Here, σ_A is standard deviation amplitude value and m_A is the mean Amplitude of a phase.

After creating the Patch, go to Matlab to process the data. To do that go to the INSAR_20210806 folder then open the terminal in this folder and type MATLAB. It opens Matlab software. Then check if the StaMPS master package is installed properly. To check simply type `help stamps`. It shows all the steps that are needed for StaMPS PSI processing.

There are 8 steps to process PSI data. These steps are-

1. Load data
2. Estimate Phase Noise
3. PS selection
4. PS weeding
5. Phase correction
6. Phase Unwrapping
7. Estimate spatially-correlated look angle error
8. Atmospheric filtering

4.2.2.1 Step -1: Load the data

In this step, convert the StaMPS export data file formats into the required file formats used for PS processing and stores the data in MATLAB. To do that in MATLAB open the command window and type (Hooper et al., 2018)

```
>> stamps(1,1).
```

4.2.2.2 Step -2: Estimate Phase Noise

This procedure consists of multiple steps. At first, it calculates and subtracts the spatially correlated phase (noise) value for each pixel in each interferogram. Then it calculates and subtracts the spatially uncorrelated DEM error for each pixel from the remaining phase. Finally, it calculated the temporal coherence for each pixel using the residual phase. To do this step type (Hooper et al., 2018)

```
>> stamps(2,2)
```

This Estimated Phase Noise step is controlled by the following parameters that shown in Table 6.

Parameter Name	Default	Description
<code>max_topo_err</code>	5	Maximum uncorrelated DEM error (in m). Pixels with uncorrelated DEM error greater

Chapter -4: Data and Methodology

		than this will not be picked (this includes error due to the phase center of the resolution element being offset from the middle of the pixel in range). Setting this higher, however, increases the mean γ value (coherence-like measure, see Hooper et al. [2007]) of pixels that have random phase.
<code>filter_grid_size</code>	50	Pixel size of grid (in m). Candidate pixels are resampled to a grid with this spacing before filtering to determine the spatially correlated phase.
<code>filter_weighting</code>	'P-square'	Weighting scheme (PS probability squared), the other possibility being 'SNR'. Candidate pixels are weighted during resampling according to this scheme.
<code>clap_win</code>	32	CLAP (Combined Low-pass and Adaptive Phase) filter window size [Hooper et al., 2007]. Together with filter grid size, determines the area included in the spatially-correlated phase estimation.
<code>clap_low_pass_wavelength</code>	800	CLAP filter low-pass contribution cut-off spatial wavelength (in m). Wavelengths longer than this are passed.
<code>clap_alpha</code>	1	CLAP α term. Together with the β term, determines the relative contribution of the low-pass and adaptive phase elements to the CLAP filter.
<code>clap_beta</code>	0.3	CLAP β term
<code>gamma_change_convergence</code>	0.005	Threshold for change in change in mean value of γ (coherencelike measure). Determines when convergence is reached and iteration ceases.
<code>gamma_max_iterations</code>	3	Maximum number of iterations before iteration process ceases.

Table 6: controlling parameters of Estimation Phase noise

Source: (Hooper et al., 2018)

4.2.2.3 Step -3: PS selection

This step selects PS based on probability and compares the findings to data with a random phase. This is frequently repeated twice. Following the first selection, the temporal coherence of each selected pixel is re-estimated more precisely by excluding the pixel from the estimation of the spatially correlated phase. Then the selection procedure is repeated. In Step 2, the pixels are selected based on the noise characteristics. but This step determines the percentage of random (non-PS) pixels in a scene, which can be used to calculate density per km2. (Hooper et al., 2018)

To run this step in MATLAB, go to the command window and type

```
>> stamps(3,3)
```

Chapter -4: Data and Methodology

The different factors that control this step of PS selection. Which are shown in this Table 7.

Parameters Name	Default	Description
<code>select_method</code>	'DENSITY'	Other option 'PERCENT'
<code>density_rand</code>	20	Maximum acceptable spatial density (per km ²) of selected pixels with random phase. Only applies if <code>select_method</code> is set to 'DENSITY'. At this stage we can usually accept a high density, as most random-phase pixels will be dropped in the next step.
<code>percent_rand</code>	20	Maximum acceptable percentage of selected pixels with random phase. Only applies if <code>select_method</code> is set to 'PERCENT'
<code>drop_ifg_index</code>	[]	Interferograms listed here (by order number given in >>ps_info) will not be included in the selection calculations

Table 7: Controlling factors of PS Point selection

Source: (Hooper et al., 2018)

4.2.2.2.4 Step -4: PS weeding

PSInSAR depends on identifying pixels that consistently reflect the radar signal over time; these are called Persistent Scatterers (PS). not all pixels are suitable for tracking ground movement. In the previous step, pixels are selected that are weeded (noisy pixels, multiple scattered pixels, non-persistent scattered pixels, etc.,). In this PS weeding step those weeded pixels are filtered out. After that, the PS pixels are stored in a different workplace.

To run this step PS weeding in MATLAB, go to the command window and type

```
>> stamps(4,4)
```

Different factors control this PS weeding step, these factors are shown in Table 8.

Parameter Name	Default	Description
<code>Weed_standard_dev</code>	1.0	Threshold standard deviation. For each pixel, the phase noise standard deviation for all pixel pairs including the pixel is calculated, If the minimum standard deviation is greater than the threshold, the pixel is dropped. If set to 10, no noise-based weeding is performed
<code>Weed_max_noise</code>	Inf	Threshold for the maximum noise allowed for a pixel. For each pixel the minimum pixel-pair noise is estimated per interferogram. Pixels whose maximum interferogram

Chapter -4: Data and Methodology

		noise value is higher than the indicated threshold are dropped.
Weed_time_win	730	Smoothing window (in days) for estimating phase noise distribution for each pair of neighbouring pixels. The time series phase for each pair is smoothed using a Gaussian-weighted piecewise linear fit. Weed_time_win specifies the standard deviation of the Gaussian. The original phase minus the smoothed phase is assumed to be noise.
Drop_ifg_index	[]	Interferograms listed here (by order number given in >>ps_info) will not be included in the weeding calculations.

Table 8: PS Weeding controlling factors

Source: (Hooper et al., 2018)

4.2.2.2.5 Step -5: Phase Correction

phase correction is a crucial step that aims to mitigate errors that introduced by different factors such as atmospheric disturbances, topographic variations, and temporal decorrelation. This phase correction process aims to enhance the accuracy and reliability of Land displacement measurement from SAR images. In this step selected pixels are corrected for spatially uncorrelated look angle (DEM) errors.

To run this step PS weeding in MATLAB, go to the command window and type

```
>> stamps(5,5)
```

Different factors control this Phase Correction step, these factors are shown in this Table 9.

Parameter Name	Default	Description
Merge_resample_size	0	Coarser posting (in m) to resample to. If set to 0, no resampling is applied.
Merge_standard_dev	inf	Threshold standard deviation. For each resampled pixel, the phase noise standard deviation is computed. If the standard deviation is greater than the threshold, the resampled pixel is dropped. Only applied in case of resampling.

Table 9: Phase Correction controlling factors

Source: (Hooper et al., 2018)

4.2.2.2.6 Step -6: Phase Unwrapping:

The phase of Synthetic Aperture Radar (SAR) data is represented as a sinusoidal wave constrained between $-\pi$ and π . This results in the interferogram being "wrapped," which means the phase values are cyclical and display discontinuities. These discontinuities appear as fringes on the map, which are depicted by arbitrary color changes. Each fringe corresponds to half the wavelength of the radar signal. For example, in the C-Band with a wavelength of 5.6 cm, one fringe represents a deformation of 2.8 cm.

Chapter -4: Data and Methodology

To utilize the produced velocity map, the interferogram must be unwrapped to show continuous phase changes. According to (Braun & Veci, 2021) Phase unwrapping involves resolving the altitude ambiguity by integrating phase differences between neighbouring pixels and then removing any integer multiple of the 2π cycle. This process results in an unwrapped image that reveals the actual continuous phase change between pixels.

The altitude of ambiguity, as defined by Ferretti et al. (2007), is the altitude difference that causes a phase change of 2π after the interferogram has been flattened. It is given by the equation (Ferretti et al., 2007). The altitude of ambiguity calculated by this equation 5

$$h_a = \frac{\lambda \times R \sin(\theta)}{2B_n} \quad 5$$

Where (h_a) is the altitude of ambiguity, (λ) is the wavelength, (R) is the range distance, ($\sin(\theta)$) is the incidence angle, and (B_n) is the perpendicular baseline.

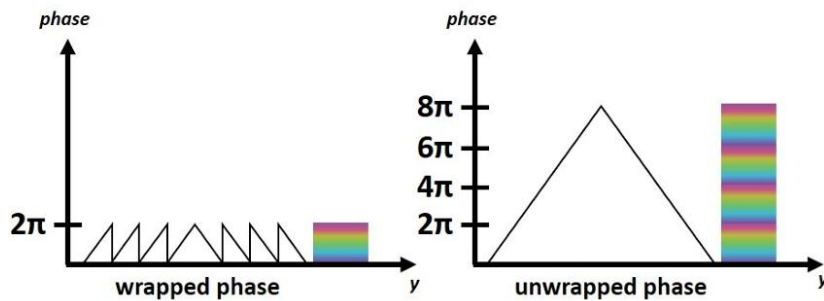


Figure 4.9: Principal of Phase Unwrapping

Source: TOPS Interferometry Tutorial by ESA

Noise in the interferogram can affect the quality of the unwrapped result. (Braun & Veci, 2021) suggests that it may be necessary to increase the signal-to-noise ratio by applying filtering techniques to improve the quality of the unwrapped phase.

The interferometric phase can be distorted by noise from temporal and geometric decorrelation, volume scattering, and processing errors. Applying the Goldstein filter, which uses Fast Fourier Transformation (FFT), can enhance the fringes in the interferogram, improving the signal-to-noise ratio for proper unwrapping. More details about this filter can be found in the publication by (Goldstein & Werner, 1998). Apply the Goldstein Phase Filtering to the de-busted image for a filtered phase image without affecting coherence. This Phase Unwrapping process happens through SNAPHU (Statistical-Cost, Network-Flow Algorithm for Phase Unwrapping). Here all the wrapped interferograms shown in Figure 4.10

Chapter -4: Data and Methodology

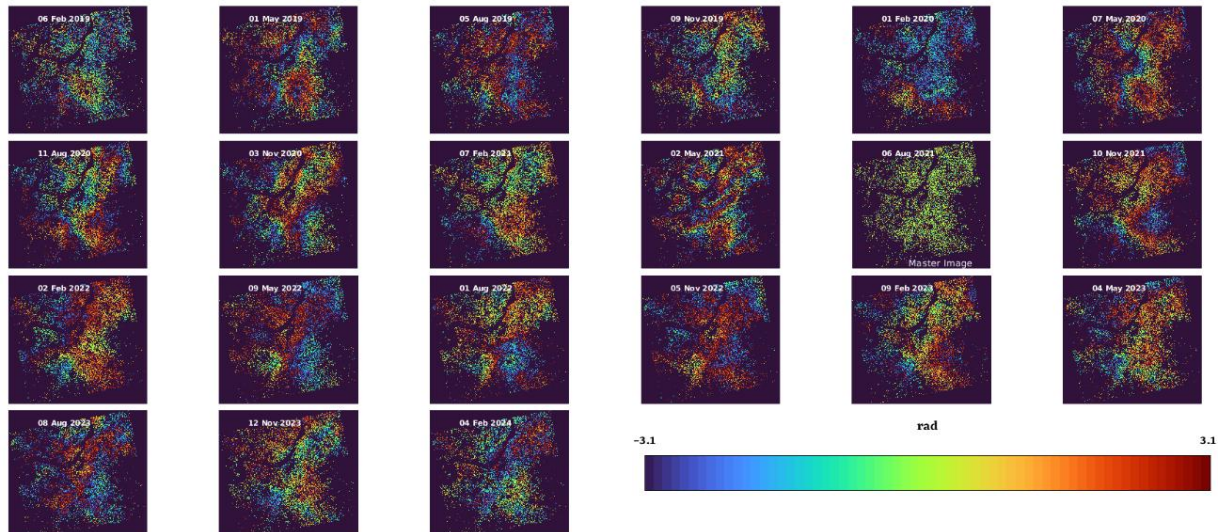


Figure 4.10: Date-wise wrapped interferograms

After phase unwrapping by SNAPHU here is all of the wrapped interferograms are smooth shown in

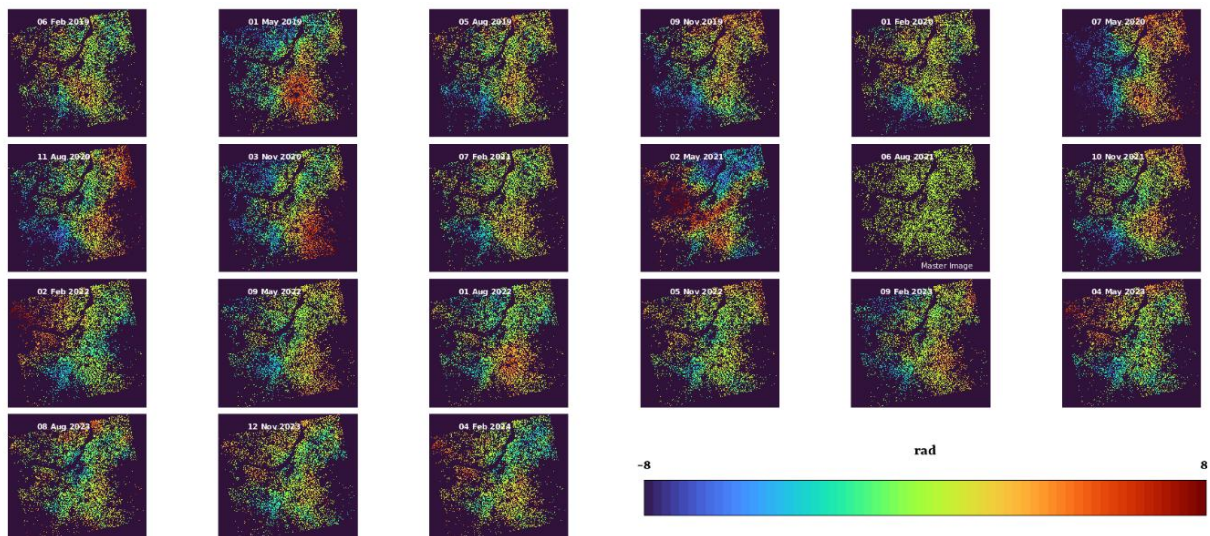


Figure 4.11: Date-wise all Unwrapped interferograms

To run this step Phase Unwrapping in MATLAB, go to the command window and type

```
>> stamps(6,6)
```

Different factors that control this Phase Unwrapping step, these factors are show in Table 10.

Parameter Name	Default	Description
unwrap_method	'3D'	Unwrapping method
unwrap_prefilter_flag	'y'	Pre-filter phase before unwrapping to reduce noise. Other option (not generally recommended) 'n'
unwrap_patch_phase	'n'	Use the patch phase from Step 3 as pre-filtered phase. If set to

Chapter -4: Data and Methodology

		‘n’ (recommended), PS phase is filtered using a Goldstein adaptive phase filter.
<code>unwrap_grid_size</code>	200	Resampling grid spacing. If <code>unwrap_prefilter_flag</code> is set to ‘y’, phase is resampled to a grid with this spacing.
<code>unwrap_gold_n_win</code>	32	Window size for Goldstein filter
<code>unwrap_time_win</code>	730	Smoothing window (in days) for estimating phase noise distribution for each pair of neighbouring pixels. The time series phase for each pair is smoothed using a Gaussian window with standard deviation of this size. Original phase minus smoothed phase is assumed to be noise, which is used for determining probability of a phase jump between the pair in each interferogram
<code>unwrap_gold_alpha</code>	0.8	Value of α for Goldstein filter.
<code>drop_ifg_index</code>	[]	Interferograms listed here (by order number given in <code>>>ps_info</code>) will not be unwrapped.
<code>subtr_tropo</code>	‘n’	When set to ‘y’, removes an estimate before unwrapping as defined using the correction in <code>tropo_method</code> . Note, this is to ease the unwrapping process, thus after unwrapping the tropospheric signals are added back in.
<code>tropo_method</code>	‘a_l’	Type of tropospheric correction that will be used to remove the tropospheric delays when <code>subtr_tropo</code> is set to ‘y’. Valid options are those supported by TRAIN (e.g. ‘a l’, ‘a e’, ‘a w’, ‘a m’, etc.).

Table 10: Phase Unwrapping controlling factors

Source: (Hooper et al., 2018)

To show the Unwrapped phase in Matlab, go to the command window and type

```
>>ps_plot ('u')
```

4.2.2.2.7 Step- 7: Estimate spatially-correlated look angle (DEM) error:

Spatially-Correlated Look Angle (SCLA) error, also known as DEM error, affects the phase measurement in PSInSAR. The study can reveal the actual deformation signal by removing the DEM error.

SCLA errors primarily arise due to inaccuracies in the Digital Elevation Model (DEM) used for PSInSAR processing. This error includes the DEM itself and incorrect mapping of the DEM into radar coordinates. In this step, the Atmospheric and Orbit Error (AOE) phase is also estimated.

To run this step Estimate Spatially-Correlated Look Angle error in MATLAB, go to the command window and type

```
>> stamps(7, 7)
```

This step is controlled by different parameters, which are shown in Table 11.

Parameter Name	Default	Description
<code>scla_drop_index</code>	<code>[]</code>	Interferograms listed here (by order number given in <code>>>ps_info</code>) will not be included in the SCLA calculations, but will still be included in Step 6 and previous steps.
<code>scla_deramp</code>	<code>'n'</code>	If set to 'y', a phase ramp is estimated for each interferogram
<code>drop_ifg_index</code>	<code>[]</code>	Interferograms listed here (by order number given in <code>>>ps_info</code>) will not be included in the SCLA calculations, nor will they be included in Step 6 and previous steps
<code>subtr_tropo</code>	<code>'n'</code>	When set to 'y', removes an estimate of the tropospheric delay as defined using the correction in <code>tropo_method</code> prior to the computation of the SCLA error
<code>tropo_method</code>	<code>'a-1'</code>	Type of tropospheric correction that will be used to remove the tropospheric delays when <code>subtr_tropo</code> is set to 'y'. Valid options are those supported by TRAIN (e.g. 'a l', 'a e', 'a w', 'a m', etc.).

Table 11: Estimate Spatially-Correlated Look Angle Error controlling factors

Source: (Hooper et al., 2018)

To display the estimate of SCLA error in Matlab, go to the command window and type

```
>>ps_plot ('d')
```

4.2.2.2.8 Step -8: Atmospheric Filtering:

Atmospheric noise is a major source of error in PSInSAR data processing. There are different types of methods available to remove the Atmospheric noise. However, the study used an advanced filtering technique called StaMPS (Stanford Method for Persistent Scatterers). This method employs a spatio-temporal filtering technique to distinguish atmospheric noise, deformation signal, and other error sources.

To run this step Atmospheric Filtering in MATLAB, go to the command window and type

```
>> stamps(8,8)
```

Chapter -5: Result and Discussion

Chapter – 5

Result and Discussion

5 Result and Discussion:

The study used 21 sentinel images with the master image dated 06 August 2021 to create 20 interferograms using the PSInSAR technique through StaMPS with integration of Matlab software. After analyzing the images, the study found that the maximum perpendicular baseline was 136 meters and the maximum temporal baseline was 924 days. While the minimum perpendicular baseline was -82 meters and the minimum temporal baseline was -912 days, as shown in **Error! Reference source not found.**. After processing PSInSAR, 81,270 PS points were generated in the Kolkata district. These points are mainly located over man-made structures such as buildings and developed areas, as these structures provide a higher coherence value compared to water bodies and vegetation. Consequently, the density of PS points over water bodies in the Kolkata District is lower, indicating the successful removal of noisy pixels in the PS-InSAR technique.

Table 12: Sentinel-1 images with their Perpendicular baseline (meters) and Temporal baseline (days) respectively.

Product	Perpendicular Baseline [m]	Temporal Baseline [days]
S1A_IW_SLC_1SDV_20210806T121240_20210806T121307_039109_049D70_A746	0	0
S1A_IW_SLC_1SDV_20240216T121249_20240216T121316_052584_065C6B_CA32	-30	924
S1A_IW_SLC_1SDV_20231112T121253_20231112T121320_051184_062C80_A5D3	40	828
S1A_IW_SLC_1SDV_20230808T121251_20230808T121318_049784_05FC98_3A5B	91	732
S1A_IW_SLC_1SDV_20230504T121246_20230504T121313_048384_05D1CD_E897	-21	636
S1A_IW_SLC_1SDV_20230209T121244_20230209T121311_047159_05A87C_E5FF	136	552
S1A_IW_SLC_1SDV_20221105T121248_20221105T121315_045759_057923_0F98	79	456
S1A_IW_SLC_1SDV_20220801T121246_20220801T121313_044359_054B39_8E67	-31	360
S1A_IW_SLC_1SDV_20220509T121240_20220509T121307_043134_0526C4_A8B4	12	276
S1A_IW_SLC_1SDV_20220202T121238_20220202T121305_041734_04F754_5A0C	120	180
S1A_IW_SLC_1SDV_20211110T121242_20211110T121309_040509_04CDC8_6104	-37	96
S1A_IW_SLC_1SDV_20210502T121234_20210502T121301_037709_047321_DF5A	78	-96
S1A_IW_SLC_1SDV_20210207T121233_20210207T121300_036484_04489D_CBF6	20	-180
S1A_IW_SLC_1SDV_20201103T121237_20201103T121304_035084_041809_D95D	17	-276

Chapter -5: Result and Discussion

S1A_IW_SLC__1SDV_20200811T121234_20200811T121301_033859_03ED25_EF2B	-81	-360
S1A_IW_SLC__1SDV_20200507T121229_20200507T121256_032459_03C246_6BBB	43	-456
S1A_IW_SLC__1SDV_20200201T121227_20200201T121254_031059_039174_4E01	16	-552
S1A_IW_SLC__1SDV_20191109T121230_20191109T121257_029834_0366F3_D352	-9	-636
S1A_IW_SLC__1SDV_20190805T121228_20190805T121254_028434_033690_415A	-25	-732
S1A_IW_SLC__1SDV_20190501T121222_20190501T121249_027034_030B64_9F80	-82	-828
S1A_IW_SLC__1SDV_20190206T121221_20190206T121247_025809_02DEE0_63AD	102	-912

5.1 PS-InSAR trend analysis without removing any error

Six zones were identified as land subsidence zones over the Kolkata district. These zones are highlighted with high subsidence values over this study area. Calculations of line-of-sight (LOS) displacement of different zones are displayed in Figure 5.1.

Table 13: Date-wise Mean LOS velocity without any error removed

Date	Upliftment	Mean Upliftment	Subsidence	Mean Subsidence
06/02/2019	19.91		-19.38	
01/05/2019	24.13		-24.89	
05/08/2019	21.45		-20.06	
09-11-20219	22.23		-19.51	
01/02/2020	17.37		-20.08	
07/05/2020	24.05		-22.34	
11/08/2020	18.54		-18.73	
03/11/2020	21.72		-20.48	
07/02/2021	16.47		-16.27	
02/05/2021	28.27		-33.61	
10/11/2021	16.15	6.38	-17.1	-7.74
02/01/2022	19.25		-20.96	
09/05/2022	19.88		-15.55	
01/08/2022	16.74		-17.92	
05/11/2022	17.29		-19.01	
09/02/2023	22.15		-18.54	
04/05/2023	20.24		-19.26	
08/08/2023	23.98		-26.89	
12/11/2023	19.01		-18.87	
04/02/2024	19.93		-21.87	

On February 6, 2019, the Kolkata district showed LOS displacement values ranging from +19.91 mm to -19.38 mm (Table) while the LOS displacement value varied from +24.13 mm to -24.89 mm (Table) on May 1, 2019. During this time, the area was significantly uplifted and also subsided. The LOS displacement value was ranging from +21.45 mm to -20.06 mm on August 05, 2019. It was noticed that the area was highly uplifted during the May to August month. On the other hand, the displacement rate was observed to +22.23 mm to -19.51 mm (Table) on November 9, 2019. Here positive values indicated the upliftment area and negative

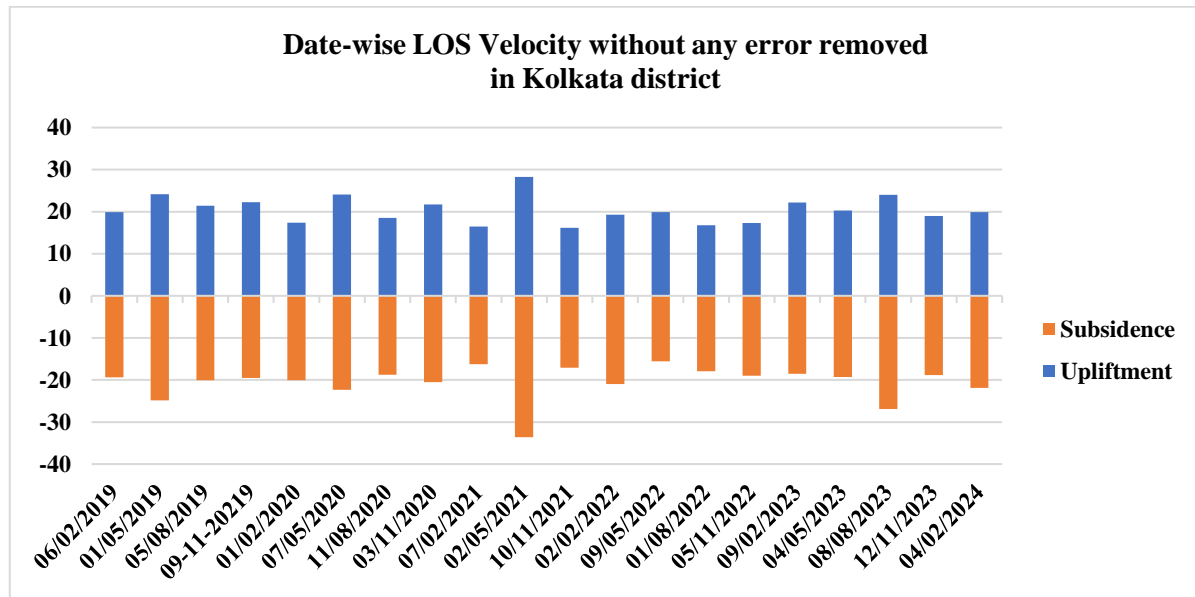
Chapter -5: Result and Discussion

value showed the land subsidence area. The blue colour was indicated the land upliftment area and also red colour represent the land subsidence area. The relative stable ground was represented in others colour such as cyan and yellow colour. Figure 5.1 is representing the land subsidence and upliftment map.

In the case of 2020, the LOS displacement rate was noticed from +24.05 mm to -22.34 mm on 1st February while +24.05 mm to -22.34 mm was identified on 7th May. On the other hand, the LOS displacement rate varied from +18.54 mm to -18.73 mm on 11th August. It was witnessed that the area was displacement in the month of May to August. The displacement rate was estimated from +21.72 mm to -20.48 mm on 3rd November over this study region. Figure 5.1 represents the land subsidence and upliftment map.

In 2021, on February 07, the Kolkata district showed LOS displacement values ranging from + 16.47 mm to -16.27 mm. On May 02, the LOS displacement value ranged from + 28.27 mm to -33.61 mm, and on November 10, the LOS displacement in the Kolkata district ranged from +16.15 mm to -17.10 mm. In 2022, the Kolkata district showed LOS displacement values ranging from +19.25 mm to -20.96 mm on 2nd February, while +19.88 mm to -15.55 mm on 9th May. Notably, the displacement rate was observed from +16.74 mm to -17.92 mm on 1st August. On the other hand, the displacement rate was estimated from +17.29 mm to -19.01 mm on 5th November. Figure 5.1 is representing the land subsidence and upliftment map.

In 2023, the displacement rate was slightly changed and ranged from +22.15 mm to -18.54 mm on 9th February, while +20.24 mm to -19.26 mm on 4th May respectively. On the other hand, the displacement area was calculated from +23.98 mm to -26.89 mm on 8th August. The LOS displacement value was observed from +19.01 mm to -18.87 mm on 12th November. On the other hand, in 2024, the LOS displacement area was noticed from +19.93 mm to -21.87 mm on 4th February. Figure 5.1 represents the date-wise LOS velocity without any error removed in Kolkata district. Figure 5.1 is representing the land subsidence and upliftment map.



Graph 5: Date-wise LOS velocity without removing any error

Chapter -5: Result and Discussion

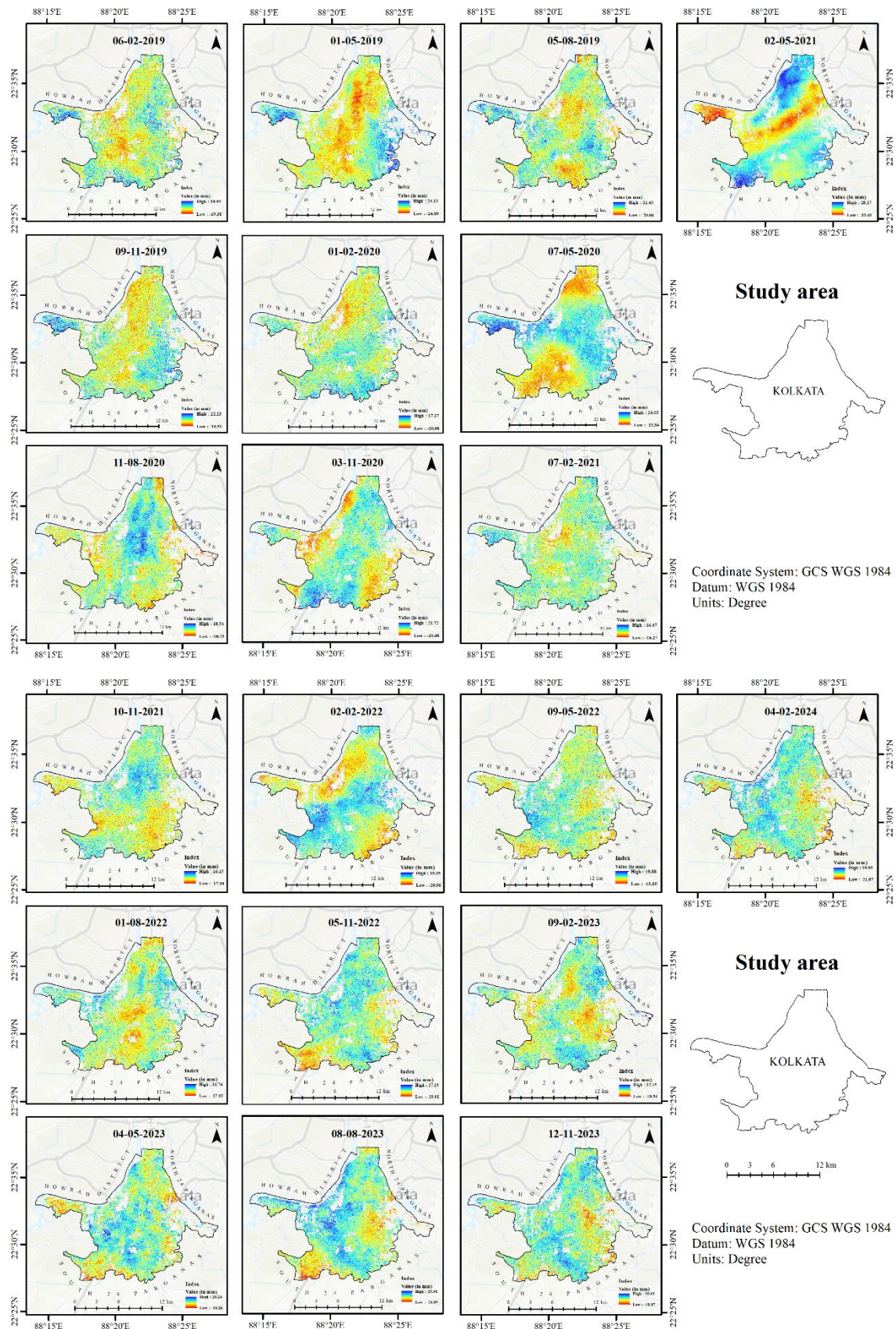


Figure 5.1: Date-wise LOS Velocity without removing any error (06-02-2019 to 04-02-2024)

Chapter -5: Result and Discussion

5.2 PSInSAR trend analysis with removing all the errors

After removing the DEM error and AEO error, the unwrapped interferograms turn smoother than the previous data. The value was slightly changed and give the proper value of unwrapped interferograms. The interferograms values were tabulated in Table 14 and showing in Figure 5.2.

Table 14: Date-wise LOS velocity value with removal of all errors like DEM error, Tropospheric error, Orbit error

Date	Upliftment	Mean Upliftment	Subsidence	Mean Subsidence
06/02/2019	19.59		-18.81	
01/05/2019	22.03		-24.16	
05/08/2019	20.56		-20.22	
09/11/2019	31.37		-19.69	
01/02/2020	16.00		-21.01	
07/05/2020	24.08		-21.87	
11/08/2020	20.43		-24.57	
03/11/2020	22.21		-20.47	
07/02/2021	16.37		-16.19	
02/05/2021	28.14		-33.53	
10/11/2021	15.97	5.00	-17.42	-5.88
02/02/2022	19.37		-20.87	
09/05/2022	20.42		-15.33	
01/08/2022	16.51		-17.15	
05/11/2022	17.96		-18.10	
09/02/2023	22.02		-18.60	
04/05/2023	20.08		-21.53	
08/08/2023	25.28		-24.20	
12/11/2023	19.14		-18.58	
04/02/2024	19.72		-21.34	

In case of 2019, highest value of upliftment rate was estimated as 31.37 mm on 9th November while high subsidence value was observed as -24.16 mm on 1st May. In 2020, the area was uplifted by 24.08 mm on 7th May, 2020 and subsided by -24.57 mm on 11th August, 2020. On the other hand, the maximum uplift area was found as 28.14 mm and -33.53 mm in 2nd May, 2021. However, peak uplift area was calculated 20.42 mm on 9th May and topmost subsidence area was identified as -20.87 mm in 2nd February in this district. During 2023-2024, it was noticed that the highest uplifted area was found as 25.28 mm, while the maximum subsidence area was -24.20 mm on 8th August, 2023. Basically, these findings suggested that the area was uplifted during rainy season (May to August) in between 2019 to 2024 due to ground recharge in clay content. Actually, this area is situated in the river bed of Ganga. It can cause the clay to expand and swell, leading to an increase in the volume of the aquifer. This expansion can exert an upward force on the overlying soil and rock layers, causing the land surface to rise. Mostly, this area was subsided due to uncontrolled and massive extraction of groundwater for domestic and industrial purposes. The upliftment and subsidence rate were representing in Figure 5.2.

Chapter -5: Result and Discussion

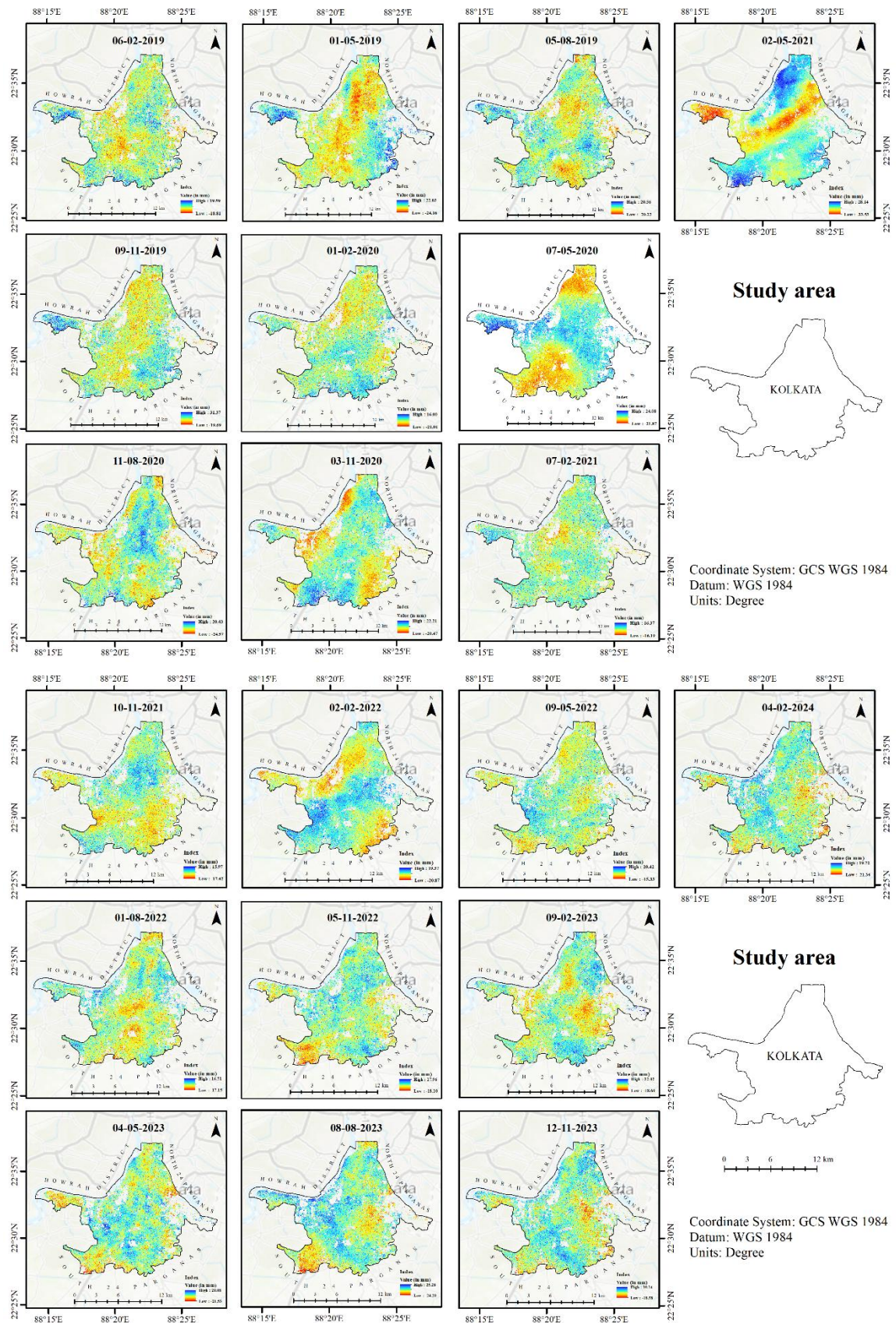
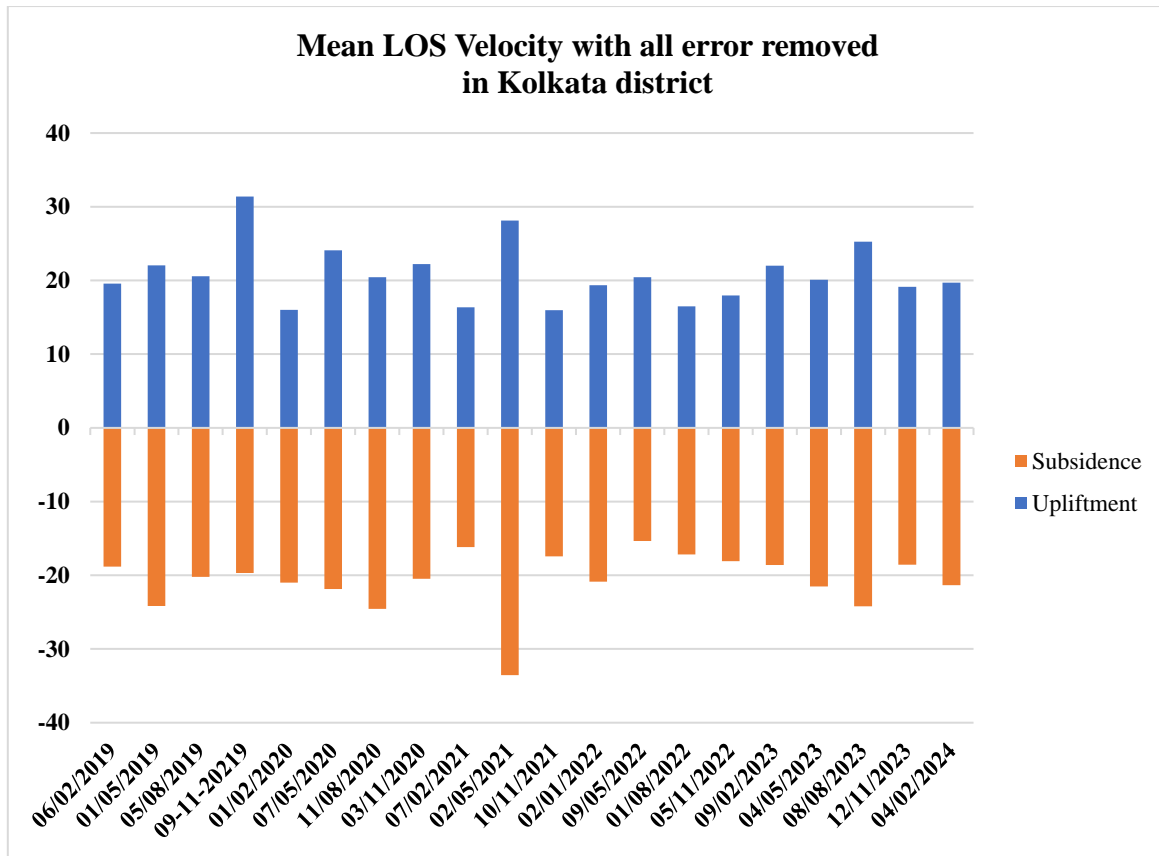


Figure 5.2: Date-wise LOS velocity with removed all type of error



Graph 6: Mean LOS velocity with all errors removed

5.3 Zone-wise land upliftment and subsidence analysis during 2019-2024

From this PSInSAR analysis, the study identified the major land subsidence area in the Kolkata district. These areas are: a) Gardenreach, b) Cossipore c) Science City d) Mukundapur e) Thakurpukur f) Barabazar, and a few other areas have also faced Land subsidence. The findings are discussed below-

a) Gardenreach:

The PSInSAR analysis revealed that the Gardeanreach area has selected 2908 Permanent Scatterer (PS) points which indicate both land subsidence and upliftment, with average rates of -5.86 mm/year and +3.83 mm/year, respectively. Here, the negative value represents the land subsidence and the positive value represents the land upliftment. These values represent the mean Line of Sight (LOS) velocity, which is the rate of ground target displacement along the radar's line of sight. The LOS value of this study area was decreasing gradually and it indicated that the area has experienced land subsidence Graph 7). The LOS direction is critical for measuring ground displacement along the radar path. On the map, red and yellow points represent areas with maximum mean LOS velocity, indicating subsidence, while blue points represent areas of land upliftment. The maximum subsidence point in Gardenreach is located at 88.26318 degrees Longitude and 22.5444 degrees latitude, and the maximum upliftment point is at 88.28057 degrees longitude and 22.55042 degrees latitude. Actually, the area is surrounded by the Ganga River in north eastern part due to this geographical location, the Gradenreach area is composed with soft sediment such as clay and silt. These types of soil are prone to settling when loads are placed on them or water levels fluctuated. On the other hand,

Chapter -5: Result and Discussion

the areas have two major road such as Frooque road and Gardenreach road. Few subsidence point was lied on these roads.

b) Cossipore:

After analyzing the Sentinel-1 image using PSInSAR and integrating it with StaMPS, the study identified 6 major areas in the Kolkata district. One of the major areas is Cossipore, where a total of 2073 PS points were found. The mean line-of-sight (LOS) velocity ranges from -4.02 mm/year to +4.93 mm/year. The negative value indicates the Land subsidence and the positive value indicates the Land upliftment. In the map, the points shown in red and yellow colours represent the locations experiencing maximum mean LOS velocity, indicating subsidence, while the blue points represent areas undergoing land upliftment. The LOS value of this study area was decreasing gradually and it indicated that the area has experienced land subsidence (Graph 7). The maximum mean LOS subsidence is located at 88.38893 degrees longitude and 22.61168 latitude, and the maximum mean LOS upliftment occurs at 88.38242 longitude and 22.6063 latitude. Basically, this area was covered with major road such as Barrackpore Trunk road and Tala railways station.

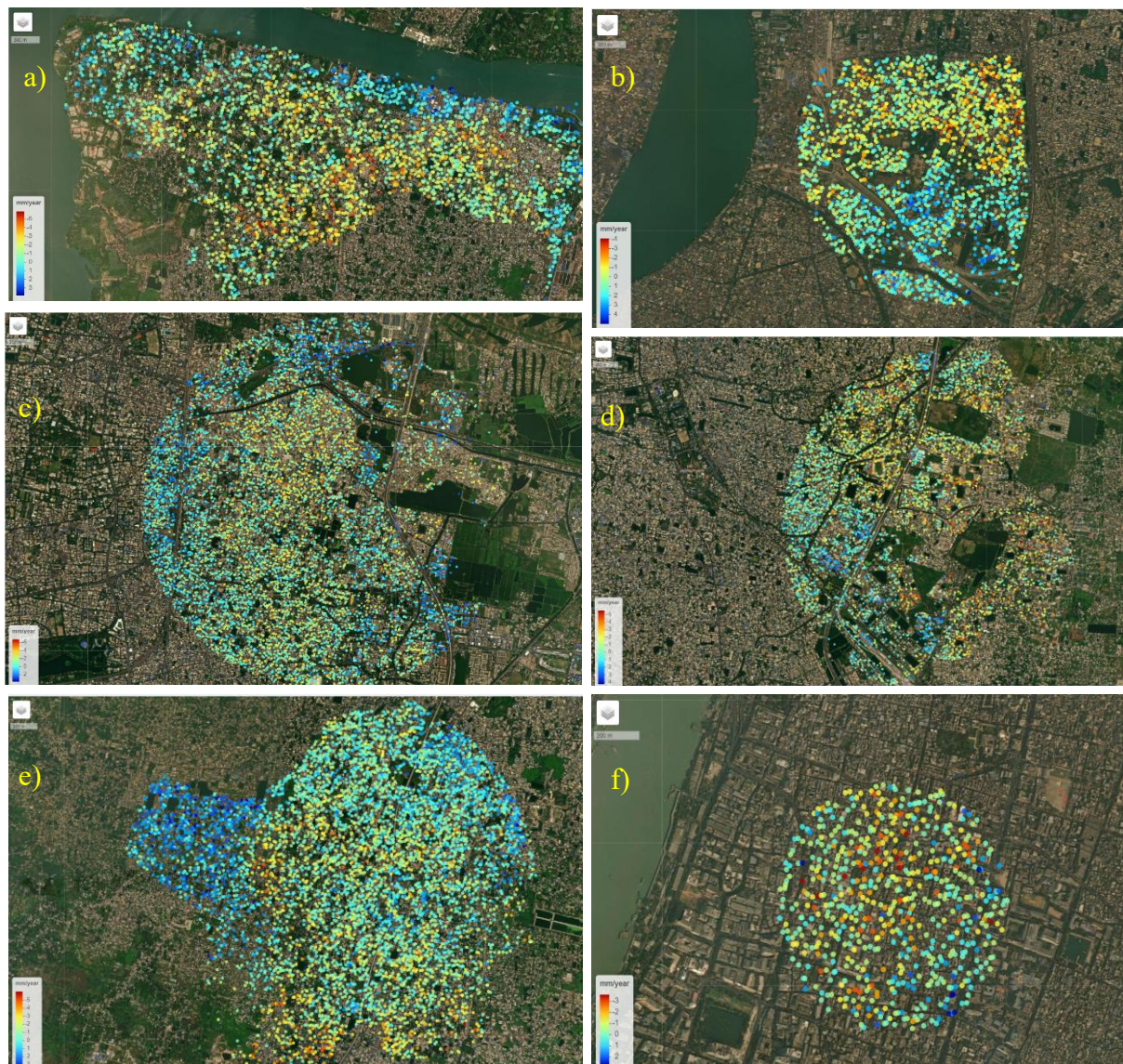


Figure 5.3: PS points of LOS velocity a) Gardenreach b) Cossipore c) Science City d) Mukundapur e) Thakurpukur f) Barabazar

Chapter -5: Result and Discussion

In eastern part of this area, Hooghly River was situated along with the area has important tank like Tala tank. The population pressure as well as rapid urbanization and construction activity are playing a major role for subsiding the Cossipore area.

c) Science City:

In the study, it was found that Science City has the highest average rate of land subsidence. The mean LOS velocity ranges from -6.86 to +3.67 mm/year. The LOS value of this study area was decreasing gradually and it indicated that the area has experienced land subsidence (Graph 7). The negative value indicates the Land subsidence and the positive value indicates the Land uplift. After analyzing the PSInSAR process, the study identified 5654 PS points in Science City. The map shows the points in red and yellow indicate locations experiencing maximum mean land subsidence, while the blue points represent areas undergoing land uplift. The coordinates for the maximum mean land subsidence are 88.39389 degrees longitude and 22.5352 degrees latitude, and the maximum mean land uplift occurs at 88.39104 longitude and 22.54202 latitude. Science City is a major town area of the Kolkata district. There is found a massive population pressure over this study region. The rapid development of urban areas such as multi-storey buildings, flat culture, and the development of road construction over there. The eastern metropolitan bypass, Bangaon-Kulpi High Road, and Picnic Garden Road are situated in this region. Major metro stations (Ritwik Ghatak Metro station, and Hemanta Mukhopadhyay Metro) are covered by this region. Few subsidence points lay on the road as well as in urban areas. The rapid exploration of groundwater used in the construction section, and for household purposes has caused to subsidence in this region.

d) Mukundapur:

Mukundapur is a significant area affected by land subsidence. The study identified 3426 PS points in this area. The mean line of sight (LOS) velocity in Mukundapur ranges from -5.55 mm/year to +4.21 mm/year. The LOS value of this study area was decreasing gradually and it indicated that the area has experienced land subsidence Graph 7. Negative values indicate land subsidence, while positive values indicate land uplift. The coordinates for the maximum mean land subsidence are 88.41327 degrees longitude and 22.48848 degrees latitude, and the maximum mean land uplift occurs at 88.38821 longitude and 22.48486 latitude. This area has two metro stations called as Jyotirindra Nandi Metro Station, Kabi Subhas Metro Station, and Bangaon Kulpi Main Road. The rapid development of urbanization is a major factor in land subsidence. The layers of soil are imbalanced as well as confined aquifer converts the neutral stress to effective stress and increases the vertical stress of the confining bed. The red and yellow colours represent the subsidence area over the study area (**Error! Reference source not found.**)

e) Thakurpukur:

Thakurpukur is a significant area affected by land subsidence. 5581 PS points were discovered in the study area. The average LOS velocity varies from -6.00 mm to +3.67 mm per year. Negative values signify land subsidence, and positive values indicate land uplift. The LOS value of this study area was decreasing gradually and it indicated that the area has experienced land subsidence Graph 7. The coordinates for the maximum mean land subsidence are 88.30135 degrees longitude and 22.45754 degrees latitude, with the maximum mean land uplift occurring at 88.29135 longitude and 22.48226 latitude. In this region, metro stations like Thakurpukur metro station, Sekher Bazar metro station, and Behala Chowrasta Metro station

Chapter -5: Result and Discussion

are situated. On the other hand, rapid growth of urbanization, population pressure, and also the groundwater is over pumped caused to land subsidence in this region.

f) Barabazar:

In the study, it was found that Barabazar has a significant amount of land subsidence. The mean LOS velocity ranges from -3.57 to +2.78 mm/year. The negative value indicates the Land subsidence and the positive value indicates the Land uplift. After analyzing the PSInSAR process, the study identified 615 PS points in Barabazar. The LOS value of this study area was decreasing gradually and it indicated that the area has experienced land subsidence Graph 7. The map shows the points in red and yellow indicate locations experiencing maximum mean land subsidence, while the blue points represent areas undergoing land uplift. The coordinates for the maximum mean land subsidence are 88.36034 degrees longitude and 22.57571 degrees latitude, and the maximum mean land uplift occurs at 88.3588 longitude and 22.57249 latitude. This area is experienced as a vital business hub of the Kolkata district. A large amount of the population is situated here. Due to the influences of the Hooghly River, the sediments are highly displaced over this region. This is a major reason for land subsidence.

Chapter -5: Result and Discussion

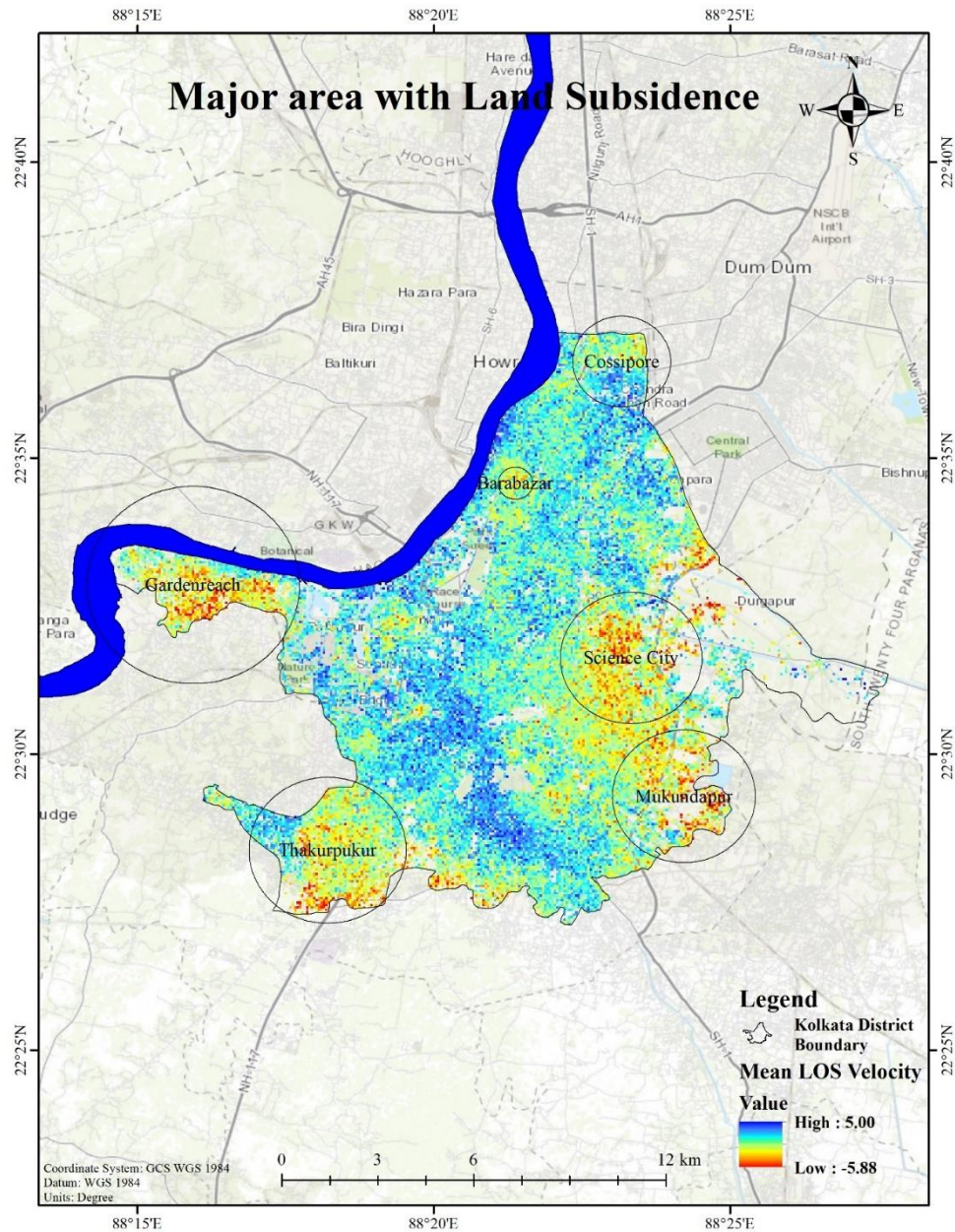
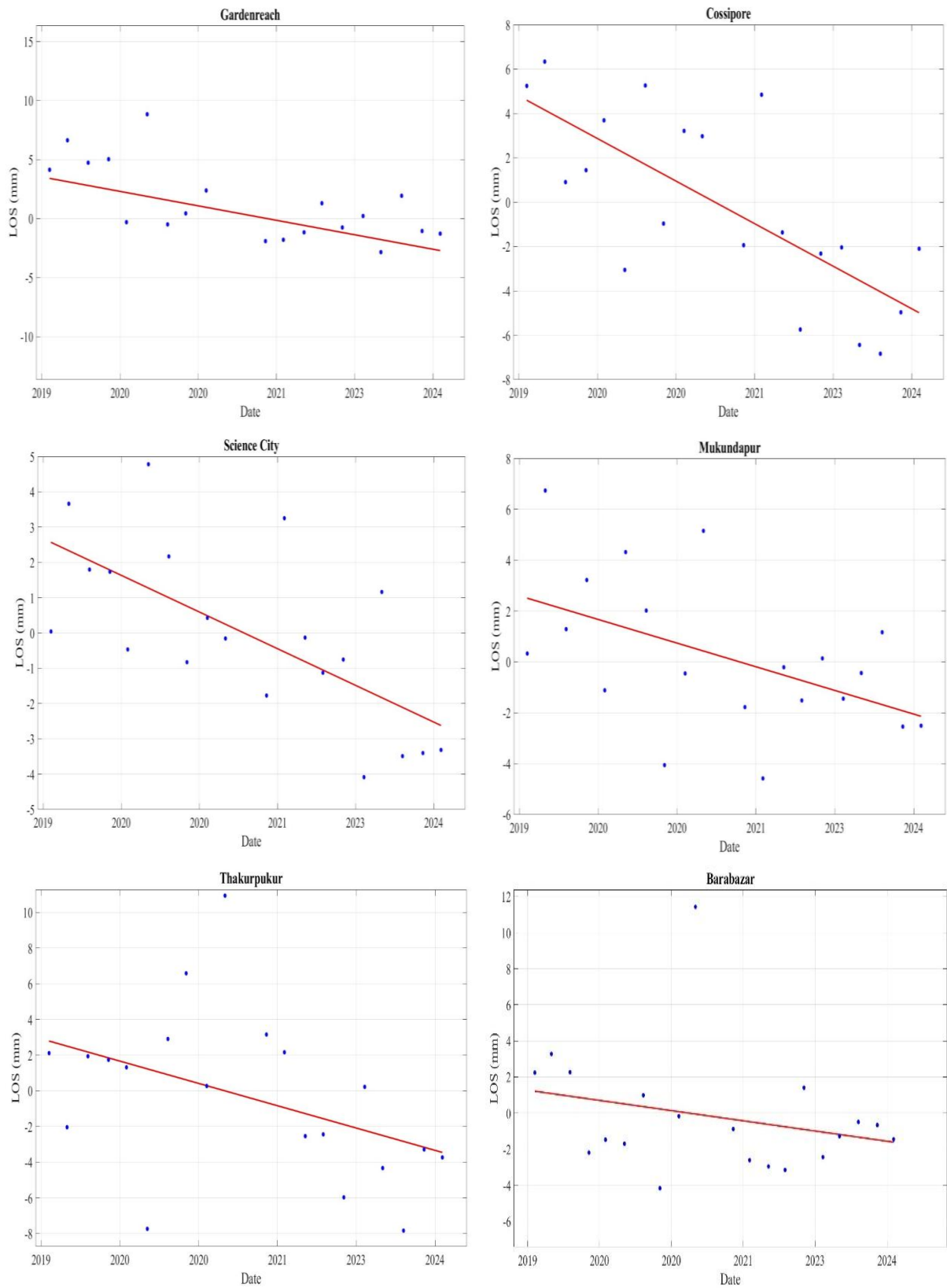


Figure 5.4: Showing the major land subsidence area in Kolkata district

Chapter -5: Result and Discussion



Graph 7: Major 6 location's LOS displacement graph

Chapter -5: Result and Discussion

Apart from these 6 Zones, several areas have detected significant Land Subsidence. These areas are Purba Barisha, Paschim Barisha, Nayabad, Dakshin Behala, Kasba, Dum Dum, Dhapa, etc. shown in this map (Figure 5.5).

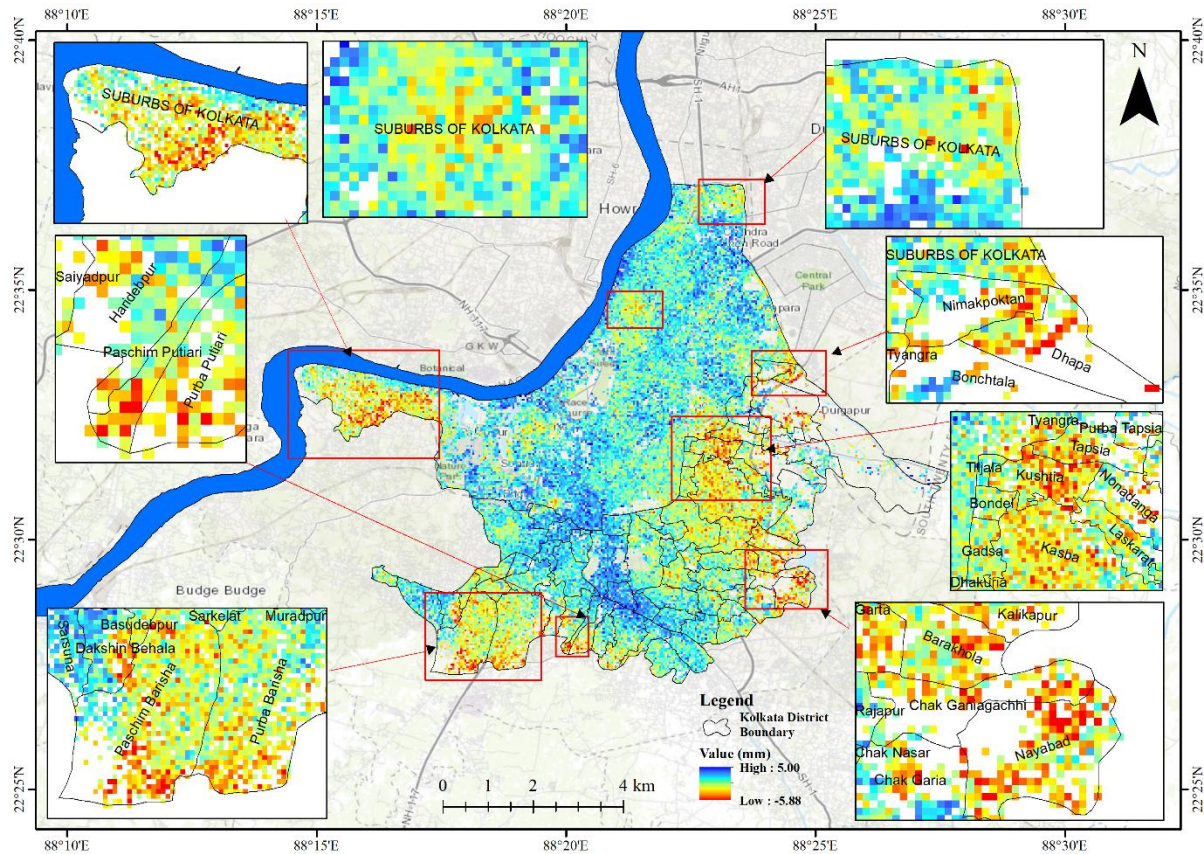


Figure 5.5: Areas in the Kolkata district where Land Subsidence detected

6 Conclusion:

This study uses the PS-InSAR approach to assess land subsidence in the Kolkata district. The most affected areas are those surrounding Garenreach, Mukundapur, Thakurpukur, Cossipore, Central, Science City, Barabazar which has a subsidence rate of approx. 5 mm/year. Apart from Salt Lake, Dum Dum, Paikpara, Dakshin Behala, Nayabad etc. The primary cause of this sinking is the uncontrolled and widespread extraction of groundwater for residential and industrial purposes. However, groundwater pumping is not the sole cause of aquifer compaction and land subsidence. Other factors such as aquifer compression based on effective stress, total stress, and pore water pressure are also significant variables in land subsidence. When groundwater is extracted, pore water pressure decreases, leading to an increase in effective stress. The primary confining bed in KMC is comprised mainly of various types of clay. This clay exhibits hysteretic behaviour, meaning it becomes stiffer upon unloading and reloading than during the initial compression. Currently, the construction of new high-rises, new roads, and excessive groundwater extraction are collectively increasing the effective stress, contributing to land subsidence. The effective porosity of the confining bed is another factor controlling the pore pressure. In the case of Kolkata, the porosity of the clay materials in the confining bed is high due to the structural arrangement of the grains, resulting in comparatively high pore pressure opposing the compression of the confining bed. Water compressibility is generally low. The highly urbanized area of KMC is affecting the infiltration of surface water into the ground. KMC is underlain by shallow-unconfined-confined types of aquifers in different places. The incidence of subsidence in KMC is controlled by the effect of head loss in unconfined and confined aquifers. Hence, the PS-InSAR method is found to be accurate, effective, and cost-efficient in identifying subsidence in urban areas by calculating subsidence from the registered vertical movement of PS points. Proper modeling considering all other factors, directly and indirectly, influencing land subsidence needs to be conducted so that KMC can understand the causes behind land subsidence more effectively.

Groundwater recharge can cause land uplift in clay deposits areas. This phenomenon is known as "land uplift due to groundwater recharge" or "groundwater-induced uplift". When groundwater is recharged into clay deposits, it can cause the clay to expand and swell, leading to an increase in the volume of the aquifer. This expansion can exert an upward force on the overlying soil and rock layers, causing the land surface to rise. In areas with thick clay deposits, groundwater recharge can lead to significant land uplift, sometimes up to several millimetres or even centimetres over time. This uplift can be gradual, occurring over years or decades, or it can be more rapid, depending on factors such as:

- The amount and rate of groundwater recharge
- The thickness and properties of the clay deposits
- The depth to the water table
- The geological history of the area

It's important to note that this process can also cause changes in soil moisture, soil chemistry, and ecosystems, and can even lead to changes in the landscape, such as the formation of new hills or valleys.

Based on existing literature, topography analysis, geological study, and also field observation, The possible reasons for land subsidence are given below-

Conclusion

The tectonic activity was observed in this study region.

Sometimes seismic activity can induce subsidence by causing ground shaking or liquefaction, particularly in areas with loose or saturated soils.

Kolkata's proximity to the Hooghly River and the coast influences subsidence through erosion, sedimentation, and tidal effects. Changes in the river courses or sea level rise can alter the hydrological conditions and impact the stability of the land.

The sediment content (clay, silty clay and) may displace according to the topographic slope. This is also a major reason for land subsidence over this reason.

Leakage from aging water and sewer pipes can soften the soil and create voids underground. Over time, these voids can lead to subsidence as the soil collapses into them, creating depression on the surface.

Reference:

- Aditiya, A., Takeuchi, W., & Aoki, Y. (2017). Land Subsidence Monitoring by InSAR Time Series Technique Derived from ALOS-2 PALSAR-2 over Surabaya City, Indonesia. *IOP Conference Series: Earth and Environmental Science*, 98(1). <https://doi.org/10.1088/1755-1315/98/1/012010>
- Ashish Aggarwal, B., & Kumar Srivastava Dharmendra Kumar Gupta Chatterjee, P. R. (2020). *PREDICTIVE MODELLING AND CHARACTERIZATION OF LAND SUBSIDENCE DUE TO GROUNDWATER AND PETROLEUM EXTRACTION IN AND AROUND MEHSANA, GUJARAT*.
- Awasthi, S., Jain, K., & Pandey, A. (2019). Psinsar Based Land Deformation Based Disaster Monitoring Using Sentinel-1 Datasets. *International Geoscience and Remote Sensing Symposium (IGARSS)*. <https://doi.org/10.1109/IGARSS.2019.8898972>
- Bagheri-Gavkosh, M., Hosseini, S. M., Ataie-Ashtiani, B., Sohani, Y., Ebrahimian, H., Morovat, F., & Ashrafi, S. (2021). Land subsidence: A global challenge. *Science of The Total Environment*, 778, 146193. <https://doi.org/https://doi.org/10.1016/j.scitotenv.2021.146193>
- Blasco, J. M. D., Foumelis, M., Stewart, C., & Hooper, A. (2019). Measuring urban subsidence in the Rome Metropolitan Area (Italy) with Sentinel-1 SNAP-StaMPS Persistent Scatterer Interferometry. *Remote Sensing*, 11(2). <https://doi.org/10.3390/rs11020129>
- Bokhari, R., Shu, H., Tariq, A., Al-Ansari, N., Guluzade, R., Chen, T., Jamil, A., & Aslam, M. (2023). Land subsidence analysis using synthetic aperture radar data. *Heliyon*, 9(3). <https://doi.org/10.1016/j.heliyon.2023.e14690>
- Bose, S., Mazumdar, A., & Basu, S. (2020). Review on Present Situation of Groundwater Scenario on Kolkata Municipal Area. *IOP Conference Series: Earth and Environmental Science*, 505(1). <https://doi.org/10.1088/1755-1315/505/1/012022>
- Braun, A., & Veci, L. (2021). *Sentinel-1 Toolbox TOPS Interferometry Tutorial*. <https://skywatch.co>
- Chatterjee, R. S., Fruneau, B., Rudant, J. P., Roy, P. S., Frison, P. L., Lakhera, R. C., Dadhwal, V. K., & Saha, R. (2006). Subsidence of Kolkata (Calcutta) City, India during the 1990s as observed from space by Differential Synthetic Aperture Radar Interferometry (D-InSAR) technique. *Remote Sensing of Environment*, 102(1–2), 176–185. <https://doi.org/10.1016/j.rse.2006.02.006>
- Chatterjee, R. S., Thapa, S., Singh, K. B., Varunakumar, G., & Raju, E. V. R. (2015a). *Detecting, mapping and monitoring of land subsidence in Jharia Coalfield, Jharkhand, India by spaceborne differential interferometric SAR, GPS and precision levelling techniques*.
- Chatterjee, R. S., Thapa, S., Singh, K. B., Varunakumar, G., & Raju, E. V. R. (2015b). *Detecting, mapping and monitoring of land subsidence in Jharia Coalfield, Jharkhand, India by spaceborne differential interferometric SAR, GPS and precision levelling techniques*.

References

- Cian, F., Blasco, J. M. D., & Carrera, L. (2019). Sentinel-1 for monitoring land subsidence of coastal cities in Africa using PSInSAR: A methodology based on the integration of SNAP and staMPS. *Geosciences (Switzerland)*, 9(3).
<https://doi.org/10.3390/geosciences9030124>
- Colesanti, C., Ferretti, A., Prati, C., & Rocca, F. (2002). *Monitoring landslides and tectonic motions with the Permanent Scatterers Technique*. www.elsevier.com/locate/enggeo
- Crosetto, M., Monserrat, O., Cuevas-González, M., Devanthéry, N., & Crippa, B. (2016). Persistent Scatterer Interferometry: A review. In *ISPRS Journal of Photogrammetry and Remote Sensing* (Vol. 115, pp. 78–89). Elsevier B.V.
<https://doi.org/10.1016/j.isprsjprs.2015.10.011>
- Davila-Hernandez, N., Madrigal, D., Exposito, J. L., & Antonio, X. (2014). Multi-Temporal Analysis of Land Subsidence in Toluca Valley (Mexico) through a Combination of Persistent Scatterer Interferometry (PSI) and Historical Piezometric Data. *Advances in Remote Sensing*, 03(02), 49–60. <https://doi.org/10.4236/ars.2014.32005>
- Ding, X., Chen, Y., Zhang, G., & Li, Z. (2014). Monitoring Earth Surface Deformations with InSAR Technology: Principle and Some critical Issues. In *Journal of Geospatial Engineering* (Vol. 2, Issue 1). <https://www.researchgate.net/publication/255607985>
- Ferretti, A., Monti-Guarnieri, A., Prati, C., Rocca, F., & Massonet, D. (2007). InSAR Principles - Guidelines for SAR Interferometry Processing and Interpretation. *ESA Training Manual*, 19.
- Ferretti, A., Prati, C., & Rocca, F. (2000). Nonlinear Subsidence Rate Estimation Using Permanent Scatterers in Differential SAR Interferometry. In *IEEE TRANSACTIONS ON GEOSCIENCE AND REMOTE SENSING* (Vol. 38, Issue 5).
- Ferretti, A., Prati, C., & Rocca, F. (2001a). Permanent Scatterers in SAR Interferometry. In *IEEE TRANSACTIONS ON GEOSCIENCE AND REMOTE SENSING* (Vol. 39, Issue 1).
- Ferretti, A., Prati, C., & Rocca, F. (2001b). Permanent Scatterers in SAR Interferometry. In *IEEE TRANSACTIONS ON GEOSCIENCE AND REMOTE SENSING* (Vol. 39, Issue 1).
- Ganguli, M. (2011). Groundwater withdrawal and land subsidence: A study of Singur Block, West Bengal, India. In *INTERNATIONAL JOURNAL OF GEOMATICS AND GEOSCIENCES* (Vol. 2, Issue 2). www.IndianJournals.com
- Goldstein, R. M., & Werner, C. L. (1998). Radar interferogram filtering for geophysical applications. *Geophysical Research Letters*, 25(21), 4035–4038.
<https://doi.org/10.1029/1998GL900033>
- Gupta, A., Asopa, U., & Bhattacharjee, R. (2019). *Land Subsidence Monitoring in Jagadhri City Using Sentinel 1 Data and DInSAR Processing*. 25.
<https://doi.org/10.3390/iecg2019-06230>
- Hooper, A., Bekaert, D., Hussain, E., & Spaans, K. (2018). *StaMPS/MTI Manual Version 4.1b*.

References

- Hooper, A., Bekaert, D., Spaans, K., & Arikan, M. (2012a). Recent advances in SAR interferometry time series analysis for measuring crustal deformation. In *Tectonophysics* (Vols. 514–517, pp. 1–13). <https://doi.org/10.1016/j.tecto.2011.10.013>
- Hooper, A., Bekaert, D., Spaans, K., & Arikan, M. (2012b). Recent advances in SAR interferometry time series analysis for measuring crustal deformation. In *Tectonophysics* (Vols. 514–517, pp. 1–13). <https://doi.org/10.1016/j.tecto.2011.10.013>
- Inaba, Y., Abe, I., Iwasaki, S., Aoki, S., Endo, T., & Kaido, R. (1970). *Reviews of land subsidence researches in Tokyo*. United Nations Educational, Scientific and Cultural Organisation. <https://policycommons.net/artifacts/10682364/reviews-of-land-subsidence-researches-in-tokyo/>
- Kadiyan, N., Chatterjee, R. S., Pranjal, P., Agrawal, P., Jain, S. K., Angurala, M. L., Biyani, A. K., Sati, M. S., Kumar, D., Bhardwaj, A., & Ray, P. K. C. (2021). *Assessment of groundwater depletion-induced land subsidence and characterisation of damaging cracks on houses: a case study in Mohali-Chandigarh area, India*. <https://doi.org/10.1007/s10064-021-02111-x/Published>
- Kampes, B. M. (2006). Radar interferometry: Persistent scatterer technique. In *Radar Interferometry: Persistent Scatterer Technique* (Vol. 12). Springer Netherlands. <https://doi.org/10.1007/978-1-4020-4723-7>
- Kandregula, R. S., G, P., Manglik, A., & Kothiyari, G. C. (2024). Estimation of surface deformation in Sikkim and Eastern Nepal Himalaya using PSInSAR technique. *Quaternary Science Advances*, 14. <https://doi.org/10.1016/j.qsa.2024.100200>
- Kumar Bhattacharya, A., & Kumar, D. (2012). *LAND SUBSIDENCE IN EAST CALCUTTA*. 2(3), 408–413. www.iosrjen.org
- Kumar, S., Kumar, D., Chaudhary, S. K., Singh, N., & Malik, K. K. (2020). Land subsidence mapping and monitoring using modified persistent scatterer interferometric synthetic aperture radar in Jharia Coalfield, India. *Journal of Earth System Science*, 129(1). <https://doi.org/10.1007/s12040-020-01413-0>
- Malik, K., Kumar, D., & Perissin, D. (2018). Assessment of subsidence in Delhi NCR due to groundwater depletion using TerraSAR-X and persistent scatterers interferometry. *Imaging Science Journal*, 67(1), 1–7. <https://doi.org/10.1080/13682199.2018.1540166>
- Meyer, F. (2019). *THE SAR HANDBOOK CHAPTER 2 Spaceborne Synthetic Aperture Radar: Principles, Data Access, and Basic Processing Techniques*.
- Mondal, A., & Paul, P. K. (2023). Monitoring of groundwater generated land subsidence by persistent scatterer analysis – A case study of the Kolkata Municipal Corporation (KMC), West Bengal. *Journal of Earth System Science*, 132(4). <https://doi.org/10.1007/s12040-023-02192-0>
- Motagh, M., Walter, T. R., Sharifi, M. A., Fielding, E., Schenk, A., Anderssohn, J., & Zschau, J. (2008). Land subsidence in Iran caused by widespread water reservoir overexploitation. *Geophysical Research Letters*, 35(16). <https://doi.org/10.1029/2008GL033814>

References

- Prati, C., Ferretti, A., & Perissin, D. (2010). Recent advances on surface ground deformation measurement by means of repeated space-borne SAR observations. *Journal of Geodynamics*, 49(3–4), 161–170. <https://doi.org/10.1016/j.jog.2009.10.011>
- Rafiei, F., Gharechelou, S., Golian, S., & Johnson, B. A. (2022). Aquifer and Land Subsidence Interaction Assessment Using Sentinel-1 Data and DInSAR Technique. *ISPRS International Journal of Geo-Information*, 11(9). <https://doi.org/10.3390/ijgi11090495>
- Rasheed, M. A., & Dayal, A. M. (2012). *Significance of Trace metal anomalies in finding hydrocarbon micro-seepage in petroliferous areas of Krishna Godavari Basin, India*.
- Raspini, F., Loupasakis, C., Rozos, D. E., Moretti, S., Raspini, F., Loupasakis, C., Rozos, D., & Moretti, S. (2013). Advanced interpretation of land subsidence by validating multi-interferometric SAR data: The case study of the Anthemountas basin (Northern Greece). *Nat. Hazards Earth Syst. Sci.*, 13, 2425–2440. <https://doi.org/10.5194/nhessd-1-1213-2013>
- Sahu, P., & Sikdar, P. K. (2011). *Threat of land subsidence in and around Kolkata City and East Kolkata Wetlands, West Bengal, India*. www.ramsar.org/brochure.html
- Sikdar, P., Biswas, A. B., & Saha, A. K. (1996). A study on the possible land subsidence in Calcutta and Howrah cities due to groundwater overdraft. *Indian Journal of Geology*, 68, 193–200.
- Suganthi, S., & Elango, L. (2020). Estimation of groundwater abstraction induced land subsidence by SBAS technique. *Journal of Earth System Science*, 129(1). <https://doi.org/10.1007/s12040-019-1298-z>
- Suganthi, S., Elango, L., & Subramanian, S. K. (2017). Microwave D-InSAR technique for assessment of land subsidence in Kolkata city, India. *Arabian Journal of Geosciences*, 10(21). <https://doi.org/10.1007/s12517-017-3207-6>
- Tomás, R., Romero, R., Mulas, J., Marturià, J. J., Mallorquí, J. J., Lopez-Sánchez, J. M., Herrera, G., Gutiérrez, F., González, P. J., Fernández, J., Duque, S., Concha-Dimas, A., Cocksley, G., Castañeda, C., Carrasco, D., & Blanco, P. (2014). Radar interferometry techniques for the study of ground subsidence phenomena: A review of practical issues through cases in Spain. *Environmental Earth Sciences*, 71(1). <https://doi.org/10.1007/s12665-013-2422-z>
- Tripathi, A., Maithani, S., & Kumar, S. (2018). *X-band persistent SAR interferometry for surface subsidence detection in Rudrapur City, India*. 28. <https://doi.org/10.1117/12.2326267>
- Walling, M. Y., & Mohanty, W. K. (2009). An overview on the seismic zonation and microzonation studies in India. In *Earth-Science Reviews* (Vol. 96, Issues 1–2, pp. 67–91). <https://doi.org/10.1016/j.earscirev.2009.05.002>
- Zebker, H. A., & Goldstein, R. M. (1986). Topographic Mapping From Interferometric Synthetic Aperture Radar Observations. In *JOURNAL OF GEOPHYSICAL RESEARCH* (Vol. 91, Issue B5).

References

Zebker, H. A., Rosen, P. A., & Hensley, S. (1997). Atmospheric effects in interferometric synthetic aperture radar surface deformation and topographic maps. *Journal of Geophysical Research: Solid Earth*, 102(B4), 7547–7563.
<https://doi.org/10.1029/96jb03804>

Zebker, H. A., & Villasenor, J. (1992). *Decorrelation in Interferometric Radar Echoes*.